ROCZNIK POLSKIEGO TOWARZYSTWA GEOLOGICZNEGO
ANNALES DE LA SOCIÉTÉ GÉOLOGIQUE DE POLOGNE

Vol. XLVIII — 2: 147—182 Kraków 1978

Irena GUCWA,[1] Tadeusz WIESER

FERROMANGANESE NODULES IN THE WESTERN CARPATHIAN FLYSCH DEPOSITS OF POLAND

(Pl. I—IV and 7 Figs)

Konkrecje żelazomanganowe w osadach fliszowych zachodnich Karpat Polski

(Pl. I—IV i 7 fig.)

Abstract: The examined ferromanganese-oxide, -carbonate and phosphate-rich nodules reveal pronounced differences in mineral and chemical composition, structure and origin. They may be classified as follows: 1 — small, goethite-todorokite-birnessite nodules of compact structure; 2 — large goethite±pyrolusite and hematite nodules of cellular structure, secondary after oligonite ones; 3 — large oligonite, Ca-rhodochrosite or mixed nodules of compact structure; 4 — small and large francolite or francolite-rhodochrosite nodules of compact structure. Trace element contents are rather low and there is no significant correlation between major, minor and trace elements (excluding Al/Cr and inconspicuous Fe/Cu interdependence).

INTRODUCTION

The hydrous ferromanganese-oxide, -carbonate and phosphate-rich nodules are not uncommon in the Flysch deposits of the Polish Caspathians. They have been reported or evidenced from different stratigraphic positions and tectonic units.

Whereas ferromanganese-oxide nodules never occur in stratiform accumulations, manganese and iron carbonates were also noticed as thin layers, e.g., of rhodochrosite composition, partly oxidized, 4 — 10 cm thick, in Eocene Variegated Shales of Magura Flysch N of Lachowice (Książkiewicz, 1958). Much more numerous and of highly varying age are examples of stratiform occurrence of siderite and of compositionally related carbonates, as recorded by Narębski (1956, 1957).

[1] Geological Institute Carpathian Branch
31-560 Kraków, Skrzatów 1 Poland

Phosphate minerals, on the other hand were, nearly exclusively, observed in the concretionary form and only in Upper Cretaceous marls (Narębski, 1958, 1960 and Jasionowicz et al., 1959). They occur as nodules of simple, or much more frequently, of mixed composition, sometimes exhibiting gradual transitions to truly ferromanganese nodules. Stratiform phosphate accumulations with much lower P_2O_5 content appear only occasionally in the Carpatian Flysch (Kamieński and Skoczylas-Ciszewska, 1955).

Except for carbonate and phosphate nodules no attempt was made to determine the chemical and mineral compositions of ferromanganese -oxide nodules of the Carpathian Flysch. The highly advanced state of knowledge of „recent" ferromanganese nodules, including, the until now much neglected carbonate ones, stimulates improvement of this situation. Another reason is the general scantiness of data concerning ferromanganese nodules generated in the geological past. Taking into account the ageing phenomena postulated even among the „recent" manganese minerals of nodules, the theoretical significance of chemical and mineral composition, as well as, of the mode of formation of Cretaceous and Palaeogene nodules of Carpathian Flysch is not without importance.

MATERIALS AND METHODS

The investigated material is consisted of samples from the collection of Prof. dr M. Książkiewicz, which were kindly transferred for examination. It embraces the samples collected during mapping of Flysch deposits and is supplemented with notices refering to location and including their stratigraphic and tectonic position (see Fig. 1). The samples with manganese content lower than 2 percent were excluded from further work, except in the phosphoria-rich nodules.

The following list of samples with preserved numeration and provided with localization and some additional data, was established basing on the chemical composition.

A. Hydrous ferromanganese-oxide nodules:

2. Harbutowice, near Sułkowice. Small (up to 6 cm in ϕ) nodule of irregular shape and columnar (external part) and earthy (internal part) structure, found in green shales corresponding to the Lgota Beds (Albian), upper part, Sub-Silesian nappe (?).

6. Ostrósza, near Ciężkowice. Nodules up to 10 cm in ϕ, irregularly shaped, with a dense and hard crust to an almost powdery and cellular interior. They occur in green shales forming intercalation in Ciężkowice Sandstone (Lower Eocene), Silesian nappe.

7. Tarnawa Górna, to S of Koźle Mt. Discoidal, up to 7 cm in ϕ, nodule is of compact structure, except for small internal cavities occurring in Variegated Shales (Palaeocene) ? (-Lower Eocene), Silesian nap-

pe. The Variegated Shales occur in the core of an anticline flanked on either side by the Oligocene Krosno Beds.

9. Lachowice, Mocznanka Creek. Irregularly shaped, up to 10 cm in ϕ nodule of cellular structure (see Pl. III, Fig. 1), from the Lower Variegated Shales (Lower Eocene), Magura nappe.

15. Lachowice. Data as for Lachowice no. 9. See also Pl. III, Fig. 2.

23. Tarnawa Dolna. Small (up. to 5 cm in ϕ), compact nodules from

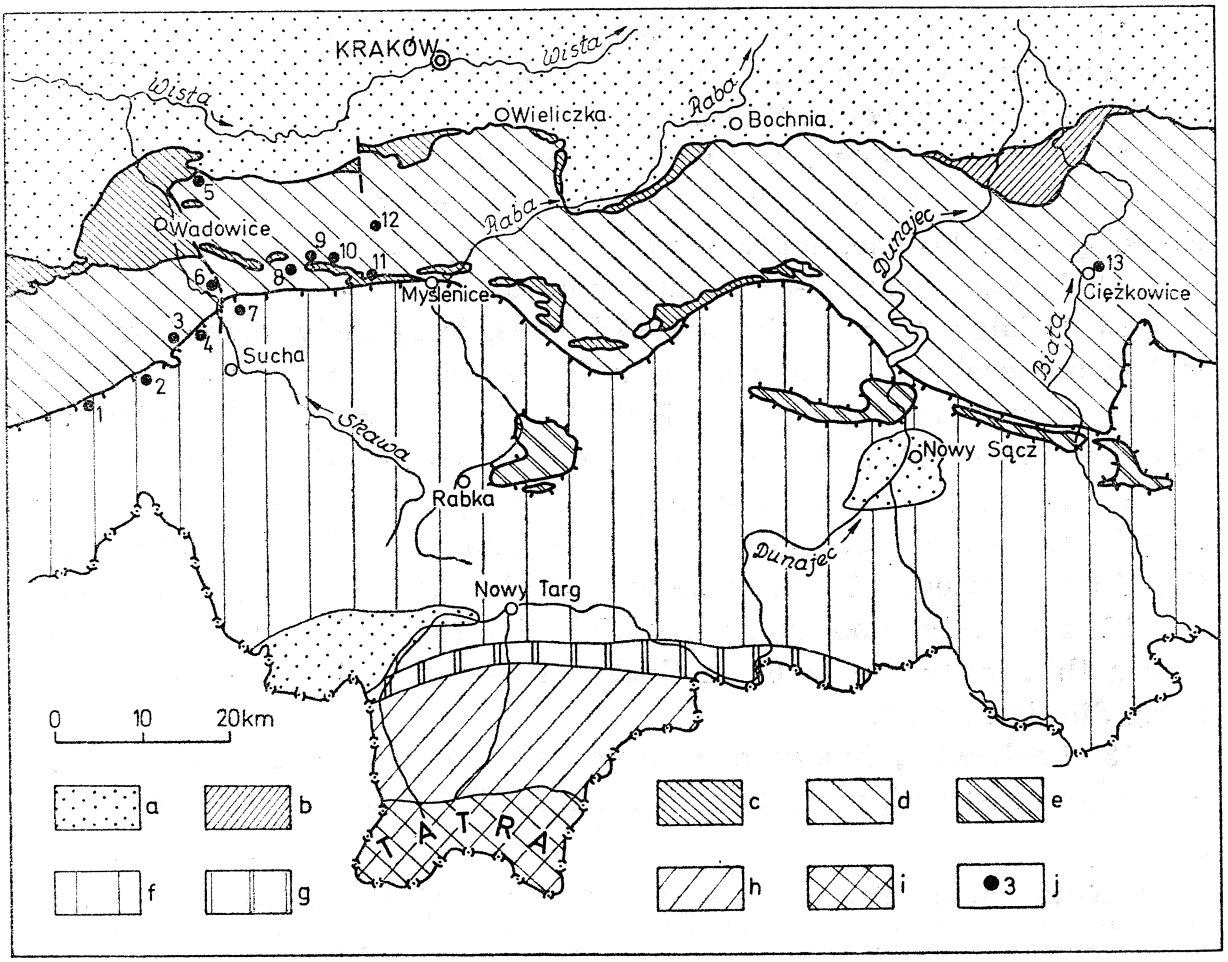

Fig. 1. Sketch-map of the examined occurrences of ferromanganese and phosphate-rich concretions in the Polish Western Carpathians (after M. Książkiewicz). a — Miocene; b — Skole nappe; c — Sub-Silesian nappe; d — Silesian nappe; e — Grybów nappe; f — Magura nappe; g — Pieniny Klippen zone; h — Podhale Flysch; i — Units of the Tatra massif; j — sites of occurrence denoted by numbers: 1 — Ślemień; 2 — Lachowice; 3 — Tarnawa Górna; 4 — Tarnawa Dolna; 5 — Lgota; 6 — Dębrówka; 7 — Zembrzyce; 8 — Działek Mt., Stronie; 9 — Lanckorona; 10 — Jastrzębia; 11 — Harbutowice; 12 — Bukowiec Mt., Rudnik; 13 — Ostrósza

Fig. 1. Mapka rozmieszczenia zbadanych wystąpień konkrecji żelazomanganowych i wzbogaconych w fosforany w Karpatach Zachodnich (według M. Książkiewicza). a — miocen; b — płaszczowina skolska; c — płaszczowina podśląska; d — płaszczowina śląska; e — płaszczowina grybowska; f — płaszczowina magurska; g — pieniński pas skałkowy; h — flisz podhalański; i — jednostki masywu Tatr; j — miejsca występowania oznaczone numerami: 1 — Ślemień; 2 — Lachowice; 3 — Tarnawa Górna; 4 — Tarnawa Dolna; 5 — Lgota; 6 — Dąbrówka; 7 — Zembrzyce, 8 — góra Działek; Stronie; 9 — Lanckorona; 10 — Jastrzębia; 11 — Harbutowice; 12 — góra Bukowiec, Rudnik; 13 — Ostrósza

the lower part of the Upper Variegated Shales (Lower Eocene, upper part), Magura nappe.

B. Phosphate-rich nodules:

22. Dąbrówka, near Skawce. Irregularly shaped, small (up to 5 cm in ϕ) and compact nodules occurring in the Variegated Shales (Lower Eocene), Silesian nappe.

25. Dąbrówka, near Skawce. Ellipsoidal, large (up to 10 cm in ϕ) and dense nodule from Hieroglyphic Beds ,Middle Eocene), Silesian nappe.

28. Tarnawa Górna, to S of Koźle Mt. Discoidal, small (up. to 4 cm in ϕ), black nodule with crust. Found in the Variegated Shales (Palaeocene (?) — Lower Eocene), Silesian nappe, see Tarnawa Górna no. 7.

29. Tarnawa Dolna. Nodules of irregular shape, large (up to 10 cm in ϕ), with inconspicuously cellular structure. From Upper Variegated Shales (Lower Eocene, upper part), Magura nappe.

C. Ferromanganese-carbonate nodules:

13. Działek, to S of Stronie. Ochreous, irregularly shaped and crustified material with compact to earthy structure in the core. It forms a thin layer (stratiform concretion?) in Menilite Shales (Eo-Oligocene), Silesian nappe. 13b and 13c. Crust and core (resp.) of sample no. 13.

16. Zembrzyce. Ash-grey, regularly ellipsoidal large (up to 12 cm in ϕ) nodule of very dense structure and conchoidal fracture. From the Upper Variegated Shales (Lower-Middle Eocene), Magura nappe.

17. Lgota. Inhomogenous material of brecciated structure constituting a thin layer (up to 6 cm thick) in Verovice Beds (Barremian-Aptian), Silesian nappe.

18. Lachowice, Mocznanka Creek. Flattened concretions, up to 15 cm in ϕ, crustified, with dense structure. They occur in the Lower Va-

---

Fig. 2. X-ray powder diagrams of selected specimens of studied nodules. Given spacings and intensities of most peculiar lines of essential minerals in the following sequence: 1 — Ostrósza 6; internal — yellow part; 2 — Ostrósza 6, red — middle part; 3 — Ostrósza 6, black — external part; 4 — Tarnawa Górna 7; 5 — Lachowice 15, internal part; 6 — Lachowice 15, peripheral part; 7 — Tarnawa Dolna 23, crust; 8 — Tarnawa Dolna 23, peripheral part; 9 — Działek 13c, internal part; 10 — Działek 13c, peripheral part; 11 — Działek 13b, crust; 12 — Dąbrówka 22; 13 — Dąbrówka 25. The letters denote the following mineral species: B — birnessite, Ca-r — Ca-rhodochrosite, F — francolite, G — goethite, H — hematite, O — oligonite, P — pyrolusite, R — rhodochrosite, T — todorokite

Fig. 2. Diagramy rentgenograficzne, proszkowe z wybranych okazów badanych konkrecji. Podano odstępy sieciowe i intensywności najbardziej osobliwych linii głównych minerałów, w następującej kolejności: 1 — Ostrósza 6, wewnętrzna część — żółta; 2 — Ostrósza 6, środkowa część — czerwona; 3 — Ostrósza 6, zewnętrzna część — czarna; 4 — Tarnawa Górna 7; 5 — Lachowice 15, część wewnętrzna; 6 — Lachowice 15, część peryferyczna; 7 — Tarnawa Dolna 23, skorupa; 8 — Tarnawa Dolna 23, część peryferyczna; 9 — Działek 13c, część wewnętrzna; 10 — Działek 13c, część peryferyczna; 11 — Działek 13b, skorupa; 12 — Dąbrówka 22; 13 — Dąbrówka 25. Litery oznaczają następujące rodzaje minerałów: B — birnessyt, Ca-r — Ca-rodochrozyt, F — frankolit, G — goethyt, H — hematyt, O — oligonit, P — piroluzyt, R — rodochrozyt, T — todorokit

riegated Shales (Lower Eocene), Magura nappe. 18a, 18b, and 18c represent wall rock, crust and core of the former samples, respectively.

19. Jastrzębia, near Izdebnik. Rather small (up to 7 cm in ϕ),

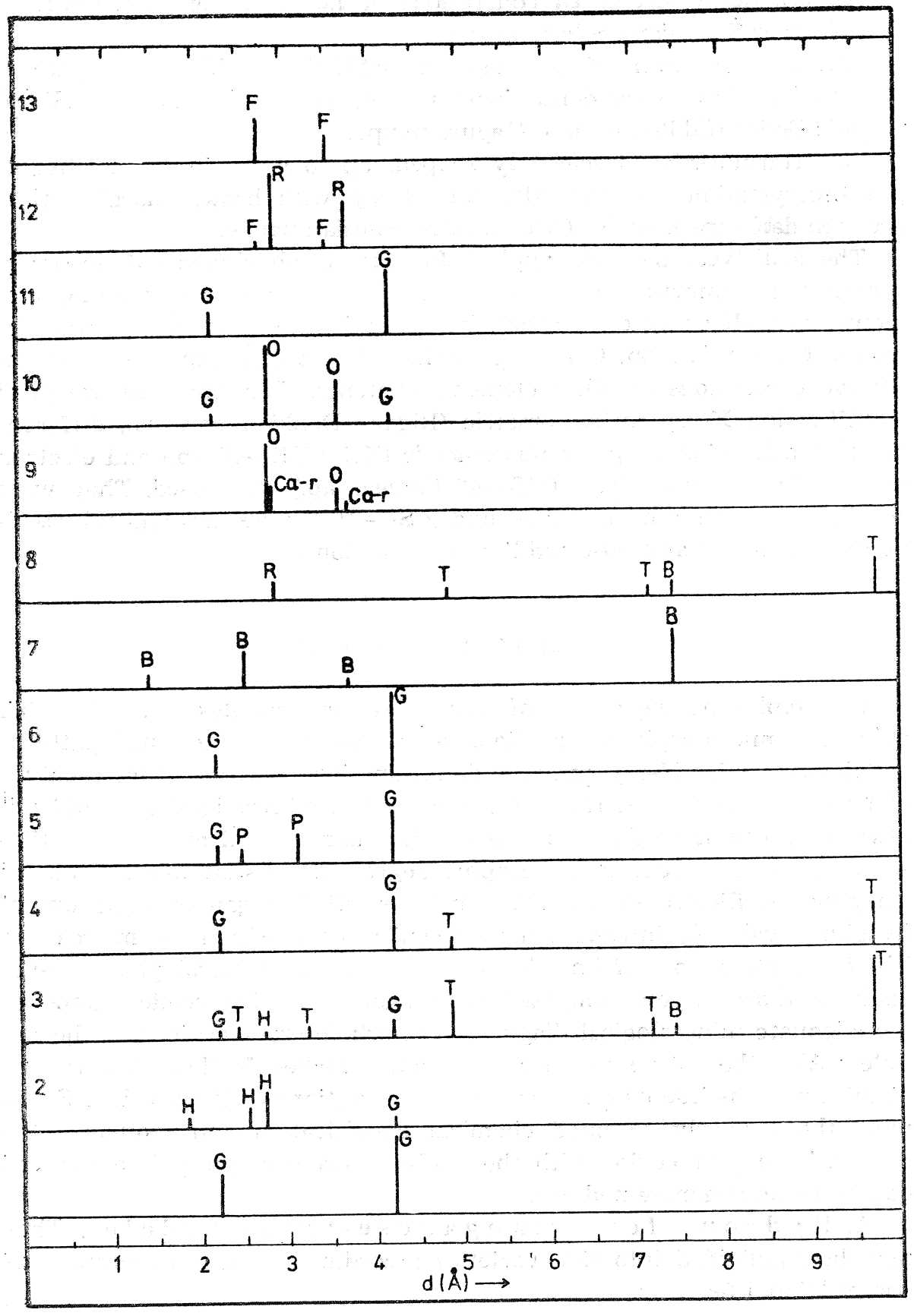

mushroom cap-shaped, crustified nodules of dense, zoned structure. In the Lower Godula Beds (Cenomanian-Turonian), Silesian nappe.

20. Bukowiec Mt., near Rudnik. Irregularly shaped, large (up to 11 cm in ϕ), dense, crustified concretions or nests in the Upper Godula Beds (Lower Senonian), Silesian nappe.

21. Ślemień, to E of Grodzisko. Crustified, discoidal nodule, up to 13 cm of ϕ, is of very dense structure and conchoidal fracture. Hieroglyphic Beds (Middle Eocene), Magura nappe.

30. Harbutowice. Irregularly shaped, up to 9 cm in ϕ, nodules of phanerocrystalline, compact structure. Grey with brown margins, they occur in dark-green shales (Albian), Sub-Silesian nappe.

The analitycal methods applied for the establishment of chemical composition comprised wet chemical analyses of major and minor elements, as well as, colorimetrical determinations of important trace elements (Cu, Co, Ni, Zn, Cr), supplemented by spectrographic semi-quantitative evaluations of other element contents. For the mineralogical identification X-ray diffractometric (Rigaku-Denki apparatus), differential thermal, infrared spectrophotometric (Zeiss UR—10 ap.) and electron microprobe X-ray analysis (MS—46 Cameca ap.) were used. They were supported by scanning electron (under S4—10 Stereoscan) and microscope in transmitted and reflected light observations.

MINERALOGY OF NODULES

In deciphering the nature of ferromanganese nodules of considerable value are microscopic observations of structural and textural patterns supplemented by X-ray mineral determinations of each single feature of texture or structure. However, those optimal investigations could not always be attainable due to much smaller than desired measures of these features or to subrentgenographic degree of crystallinity of mineral components. Electron-microprobe analyses fill this gap to some extent by giving valuable information on chemical compositions of microareas. The incomplete state of knowledge of the present mineral phases, especially of those largely composed of manganese oxides, renders impossible adequate mineralogical diagnostics of whole cross-sections of the nodules. Also the softness of fragile nodules makes further observations of mineral constituents on poorly polished sections of little value. Following the formerly accepted chemical classification and sequence, the descriptional part begins with the study of predominantly hydrous and oxidic ferromanganese nodules.

A. Hydrous ferromanganese-oxide nodules. They may be subdivided into five varieties according to their structural and compositional features.

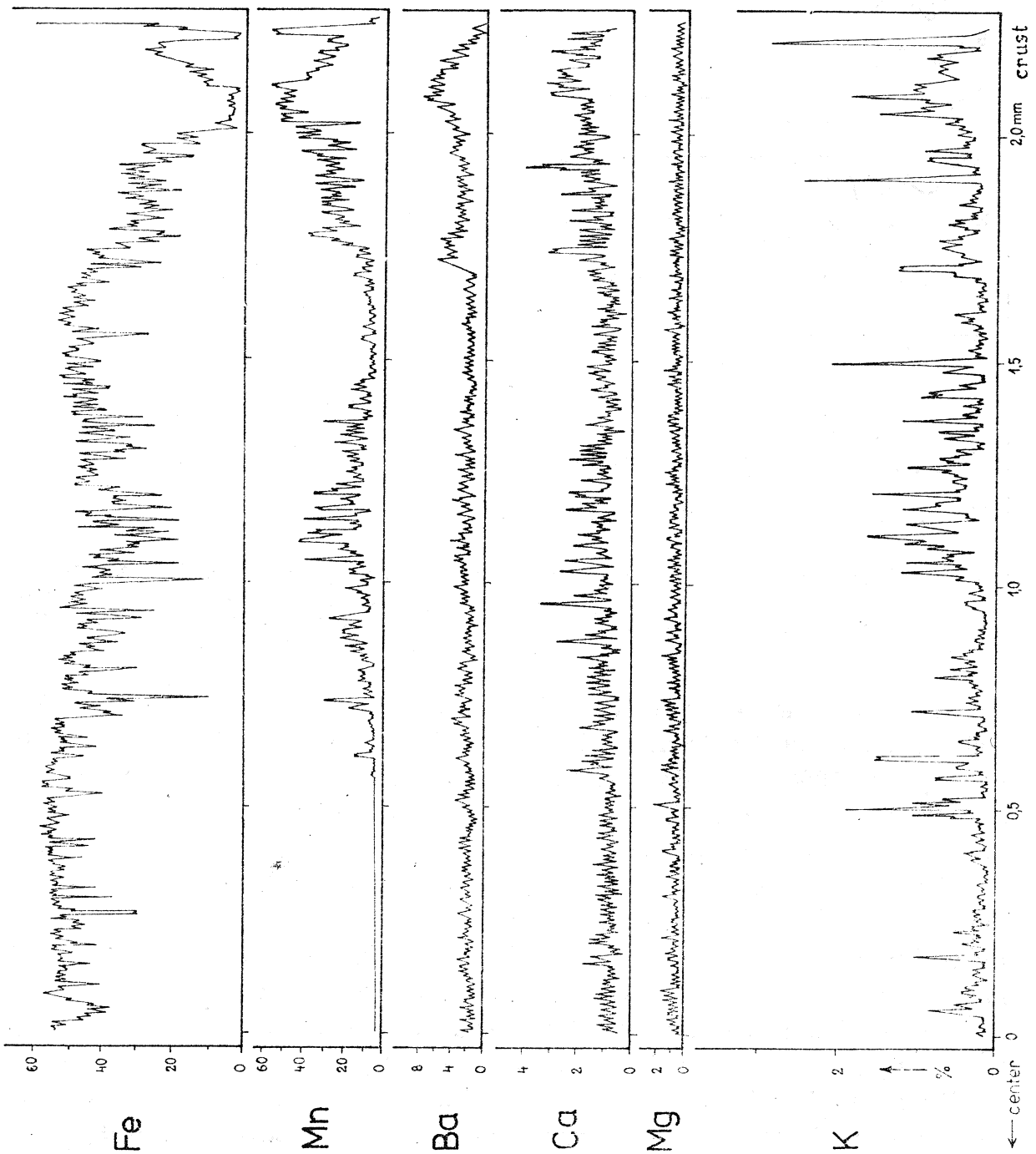

Fig. 3. Electron microprobe X-ray scans demonstrating Fe, Mn, Ba, Ca, Mg and K distribution in profile (2.2 mm in length) from the external part of the Tarnawa Górna 7 ferromanganese-oxide nodule. The rather irregular curves are due to increased recorder sensitivity

Fig. 3. Szczegółowe badania mikroanalizatorem rentgenowskim obrazujące rozmieszczenia Fe, Mn, Ba, Ca, Mg i K w profilu (2,2 mm długości) w zewnętrznej części konkrecji żelazomanganowo-tlenkowej z Tarnawy Górnej 7. Stosunkowo nieregularne krzywe spowodowała podwyższona czułość registratora

The first variety, comprising Harbutowice 2 sample, has an irregular shape and shows compact and columnar structure in the brownish black outer part and powdery to earthy structure and yellowish brown hue in the core. In both modifications peculiar lines of X-ray patterns infer the presence of goethite alone, as in the yellow part of the Ostrósza 6 nodule (Fig. 2,1). On the other hand, DTA graph (Fig. 4) of the

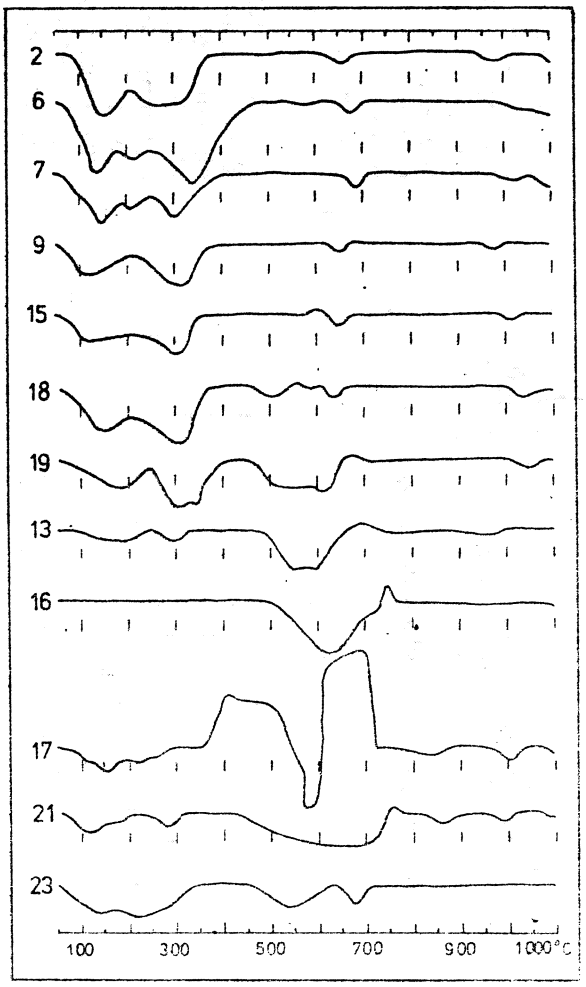

Fig. 4. DTA graphs of ferromanganese--oxide and -carbonate nodules. Recorded numerals follow the numeration of samples adopted in text

Fig. 4. Wykresy DTA dla żelazomanganowych konkrecji tlenkowych i węglanowych. Podane cyfry są zgodne z numeracją próbek przyjętą w tekście

whole sample demonstrates endothermic reactions in the range of 640—650° and 960—970°C, diagnostic for pyrolusite (Kulp and Perfetti, 1950; Ljunggren, 1960), in addition to goethite, endothermic reactions prove a large content of adsorbed water (hydrogoethite). The secondary nature of this nodule is quite probable.

The second variety, represented by indisputably secondary nodules, embraces the samples from Lachowice 9 and 15. They are distinguished by cellular structure (see Pl. III, Fig. 1 and 2). The cell walls of these large and irregularly shaped nodules consist of symmetrically distributed zones of pyrolusite ± goethite (Fig. 2,5), hematite + geothite (Fig. 2, like 2), and goethite (Fig. 2,6), well discernable due to different reflectivity on polished sections. They originated from metasomatic veinlets connected with contractional fractures in formerly carbonate (oligonite)

nodules, as shown in Fig. 1, Pl. I. During the second stage of alteration, the carbonate leaching processes predominated over oxide deposition, leading to the formation of cell walls. In the last stage, the interiors of the cells became partly filled with hydrogoethite and pyrolusite (detectable only by DTA techniques, Fig. 4), taking the shape of colloform aggregates with botryoidal surfaces.

Fig. 5. DTA graphs of phosphate-rich ferromanganese nodules. Numerals of samples as in text

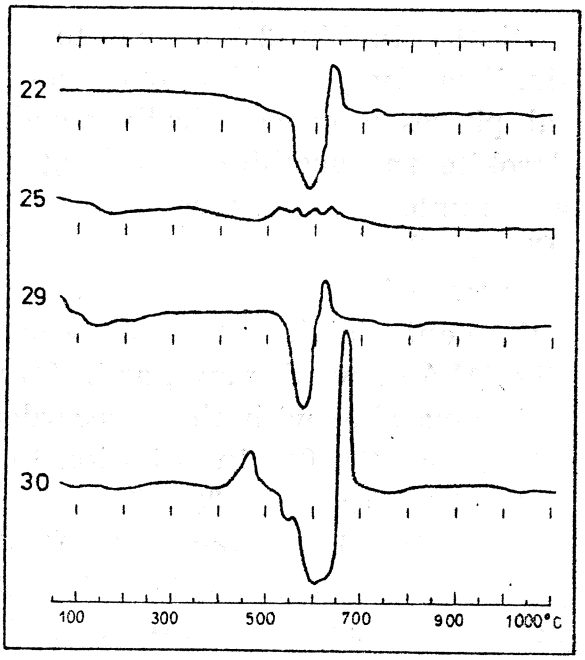

Fig. 5. Wykresy DTA dla bogatych w fosforany konkrecji żelazomanganowych. Cyfry dla próbek jak w tekście

The third variety, represented only by samples from Ostrósza (6), displays some similarity marks to the former and following varieties. The samples exhibit a conspicuous zonal distribution of minerals and cavernous structure with cavities of quite small dimensions and without secondary infillings. Mineralogically they differ in comperison with the Lachowice 9 and 15 samples by the appearance of „manganous manganite" minerals, like todorokite and rarer birnessite. These two minerals with abundant goethite and scarce hematite are the essential mineral phases composing the brownish black, thick and compact, marginal parts of nodules, as evidenced in bar diagram (Fig. 2,3) and DTA graph (Fig. 4). The middle, red part distinguishes chiefly earthy or powdery hematite with subordinate goethite (Fig. 2,2), while the innermost, yellow part is monomineralic with powdery hydrogoethite as the only mineral constituent (Fig. 2,1). The scanning electron micrographs (Fig. 3—6, Pl. IV) revealed that todorokite shows a fibrous habit of crystallites, judging from well developed fibers, straight or slightly curved, dispersed or forming clusters on the fracture surfaces in the external part of nodules. Fibrous and soft todorokite, partly due to difficulties in obtaining good polished sections, show poor reflectivity, signs of anisotropism and wavy extinction when observed by means of polarizing microscope. The same habit of crystallites seems to exhibit another MnO_2 — rich

mineral — birnessite (see Jones and Milne, 1956) the formula of which is: $(Na_{0.7}\ Ca_{0.3})\ Mn_7O_{14}\ .\ 2.8H_2O$. This mineral forms interstitial matrix showing much poorer crystallinity.

The fourth variety, the most abundant, known from Tarnawa Górna 7 and Tarnawa Dolna 23 occurrences, distinguished by its almost black colour, compact structure and its occasionally present, small contractional cavities. The nodules from the first locality, as evidenced diagrammatically in Fig. 2,4 belong to the simple association of todorokite, insignificantly prevailing over goethite. The distribution of these mineral phases is concentrically zonal. The marginal part, representing todorokite and goethite assemblage, shows a specific distribution of major and minor elements as indicated by electron microprobe X-ray scans (Fig. 3). The much advanced Ca, Ba and K substitution in „manganous manganite" phase interlayers, normally attributed to the low steric requirements (high lattice tolerance) of this phase, is well demonstrated. The DTA curve displays, as in Ostrósza 6 sample, endothermic peaks more comparable with those recorded by Straczek et al. (1960) than by Ljunggren (1960). In addition to the two goethite peaks in the range 100—150° and 250—300°C, three endothermic reactions connected with dehydration, breakdown into Mn_2O_3 and Mn_3O_4 may be traced at temperature ranges 200—230°, 660—680° and 980—990°C. The last mentioned two peaks are situated at a little higher temperatures than those of pyrolusite and correspond to reported by Frondel et al. (1960) for todorokite. The X-ray data for this mineral tabulated in Table la are well comparable with those obtained for samples from Ostrósza 6 and Tarnawa Dolna 23, as well as, with those published by above mentioned authors. Taking into account the bimineralic association in the analyzed Tarnawa Górna 7 nodule (see Table 2a) the following approximate crystallochemical formula of todorokite may be calculated after elimination of quartz, clay mineral and goethite admixtures and taking into account the results of spectrographic determinations of Ba and Sr:

$$(Ca_{0.20}Na_{0.08}K_{0.07}Ba_{0.03}Sr_{0.03}Mn^{2+}_{0.59})\ (Mn^{4+}_{4.89}Mn^{2+}_{0.75}Mg_{0.18})_{5.79}O_{12}.3H_2O$$

This formula is in good agreement with those reported by Frondel et al. (1960) and Straczek et al. (1960):

$$(Mn^{2+}, Mg, Ca, Ba, K, Na)_2\ Mn^{4+}_5O_{12}.3H_2O$$

and $(Ca, Na, Mn^{2+}, K)\ (Mn^{4+}, Mn^{2+}, Mg)_6O_{12}.3H_2O$, respectively.

The fifth variety was detected among samples from Tarnawa Dolna 23. Except representatives of the fourth variety there are available nodules which contain goethite with todorokite, the more oxidized birnessite and non-oxidized oligonite and Ca-rhodochrosite. The first Mn-

Table - Tabela 1a

X-ray data of minerals of the ferromanganese-oxide nodules: Cu K_α radiation, Ni filter

Dane rentgenograficzne minerałów konkrecji żelazistomanganowo-tlenkowych: promieniowanie Cu K_α, filtr Ni

Ostrósza 6		Tarnawa Górna 7		Tarnawa Dolna 23	
d (Å)	I/I_o	d (Å)	I/I_o	d (Å)	I/I_o
Todorokite		**Todorokite**		**Todorokite**	
9.62-9.70	2 b	9.60-9.71	2.5 b	9.60-9.71	1 b
6.93-7.03	1 b	7.18	1	7.07	1
4.82	2	4.81	1.5	4.76-4.87	2
4.45	1 b	4.4-4.5	1 b	4.45	1 b
3.47	1.5	3.47	0.5	3.20	0.5
3.201	1	3.206	1	2.45	0.5 b[1]
2.46	3 b[1]	2.46	5 b[1]	2.38-2.39	1 b
2.378	1	2.390	0.5	**Birnessite**	
2.335	0.5	2.338	0.5	7.25-7.46	4 b
2.225	0.5 b[1]	2.21	2 b[1]	3.6-3.7	1 b
1.977	1[2]	1.977	1[2]	2.41-2.47	2.5 b[2]
1.725	0.5	1.726	1		
1.667	0.5[1]	1.667	1[1]		
1.541	0.5[1]	1.54	1 b[1]		
Birnessite		**Goethite**			
7.33	1	4.165	6		
3.69-3.70	2	3.36	2 b[3]		
2.45	3 b[2]	2.685	3		
Pyrolusite		2.572	1		
3.123	3	2.475	1		
2.412	1.5	2.45	5 b[3]		
2.099	1	2.255	1		
1.628	2	2.21	2 b[3]		
1.554	1	2.175	2		
Goethite		1.907	1		
4.13-4.17	3 b	1.812	2		
2.688	4	1.718	2.5		
2.189	2	1.688	2		
1.716	1 a.o.	1.646	1		
Hematite		1.566	1		
3.65-3.67	1				
2.695	2				
2.513	1.5				
1.837	1				
1.688	3[4]				

1- coincidence of todorokite with goethite ± quartz,
2 - coincidence of birnessite with goethite ± quartz,
3 - coincidence of goethite with quartz ± todorokite,
4 - coincidence of hematite with goethite,
b - broad

mineral is confined to the peripheral part (Fig. 2,8 and Table 1a) and is replaced by birnessite in the crust (Fig. 2, 7), while the carbonate minerals tend to concentrate with goethite only in the core of the nodules (see Fig. 4, no. 23). The X-ray diffraction patterns of birnessite are comparable with those found for the same mineral in the Ostrósza 6 sample (Table 1a). The relatively high dispersion of minute birnessite crystallites in the nodule crust is responsible not only for broadening of X-ray lines but also causes the appearence of brown instead of black colour. For the same reason birnessite is brown in transmitted light. The optic properties in reflected ligth are undeterminable owing to poor quality of polished sections.

B. Phosphate-rich nodules. Two varieties of phosphoria-rich nodules might be distinguished, namely, carbonate-poor and carbonate-rich. Except these quantitative differences, another reason of this classification, is their carbonate composition.

Carbonate-poor variety, represented by specimens from Dąbrówka 25 and Tarnawa Górna 28, exhibit more compact structure than displayed by the carbonate-rich varieties. In the first mentioned, Dąbrówka 25 samples, the carbonate grains appear in the from and texture of sherulites 0.04—0.13 mm in diameter. As follows from optical and X-ray data interplanar spacings and cell parameters they consist of manganiferous siderite. Less frequent is calcite in larger grains but undetectable in DTA graph (Fig. 5) and siderite. Kaolinite, quartz and hydromuscovite are detritic minerals dispersed in a dense phosphate matrix. The phosphate mineral is identical in the whole sample. It is represented by francolite with c/a ratio = 0.7391, determined after Brasseur's (1950) method. The Tarnawa Górna 28 samples display normally in its X-ray patterns the association of francolite with quartz (see Table 1b) as in some samples from Dąbrówka 25 (Fig. 2,13; quartz excluded as in all bar diagrams). However, microscopic observations allow the detection of some small amounts of additional detritic hydromuscovite, glauconite and diagenetic Fe-septechlorite. The last mineral being accompanied by chalcedony and francolite, fills sometimes the Radiolaria frustule interiors. Numerous spicules, agglutinated Foraminifera tests and burrowing traces are also present. The mean c/a ratio of francolite equals 0.7383 and this value is distinctly smaller than in the former case. This may be considered to be due to a decrease in the content of CO_3 radicals or an increase of fluor anion share. The francolite prisms from cores of Radiolaria frustules, reaching 8 μm in length, display an elongation ratio = 1 : 2—3 and refractive index, $n\omega = 1.619 — 1.620$.

The carbonate-rich phosphate nodules from Dąbrówka (22) and Tarnawa Dolna (29) characterizes the mineral assemblage comprising francolite and rhodochrosite as the essential minerals (Fig. 5 and Table 1b). Small differences persist only in subordinate mineral combinations; qua-

rtz and kaolinite being peculiar for the first specimen and goethite with Fe-septechlorite — for the second. Rhodochrosite crystal habit is long-ovaloidal or spindle-shaped with elongation ratio = 1 : 6—7 and the

Table - Tabela 1b

X-ray data of minerals of the phosphate-rich nodules:
Cu K_α radiation, Ni filter

Dane rentgenograficzne minerałów konkrecji bogatych w fosforany: promieniowanie Cu K_α, filtr Ni

Tarnawa Górna 28		Tarnawa Dolna 29		Dąbrówka 22	
d(Å)	I/I_o	d(Å)	I/I_o	d(Å)	I/I_o
Francolite		Francolite		Francolite	
3.445	1	2.798	1.5	3.451	0.5
2.795	4.5	2.706	1	2.790	3
2.701	2.5	2.24	0.5[1]	2.700	1
2.631	1	2.13	1[1]	2.624	0.5
2.28	1[1]	Rhodochrosite		2.24	1[1]
2.24	1.5[1]	3.6627	2	Rhodochrosite	
2.13	1.5[1]	2.8488	3	3.6596	3
1.884	0.5	2.3895	1	2.8480	7
1.8397	1.5	2.1750	1	2.3892	2
1.7932	1	1.9990	1.5	2.1746	2
1.7676	0.5	1.831	0.5[2]	1.9992	2
1.7459	0.5	1.764	1[2]	1.8313	1.5[2]
1.7233	0.5	Goethite		1.7695	3.5[2]
Quartz		4.168	1 a.o.	Quartz	
4.255	2	Fe-chlorite		4.255	0.5
3.343	5 a.o.	3.483	2 a.o.	3.343	3 a.o.
				Kaolinite	
				7.13	1 a.o.

[1] - coincidence of francolite with quartz
[2] - coincidence of rhodochrosite with francolite

length, either up to 0.06 or up to 0.09 mm, respectively. The calcite molecule admixture in manganese carbonate, established (Fig. 6) from $d_{10.4}$ = 2.8400 to 2.8488 Å and $d_{01.2}$ = 3.6596 to 3.6027 Å latiice spacings, implies similar, very small $CaCO_3$ content amounting 0.5—1 percent, respectively. Rhodochrosite may be partly oxidized, especially if filling burrowing traces (Plate II, Fig. 2). The francolite from the corresponding samples yielded uncertain values of c/a ratio owing to coincidence of some reflections with those given by rhodochrosite.

C. Ferromanganese-carbonate modules. The most variable in composition and simultaneously the most frequent are the no-

dules composed of iron and manganese carbonates. As in the formerly described varieties there are examples of nodules of mixed composition.

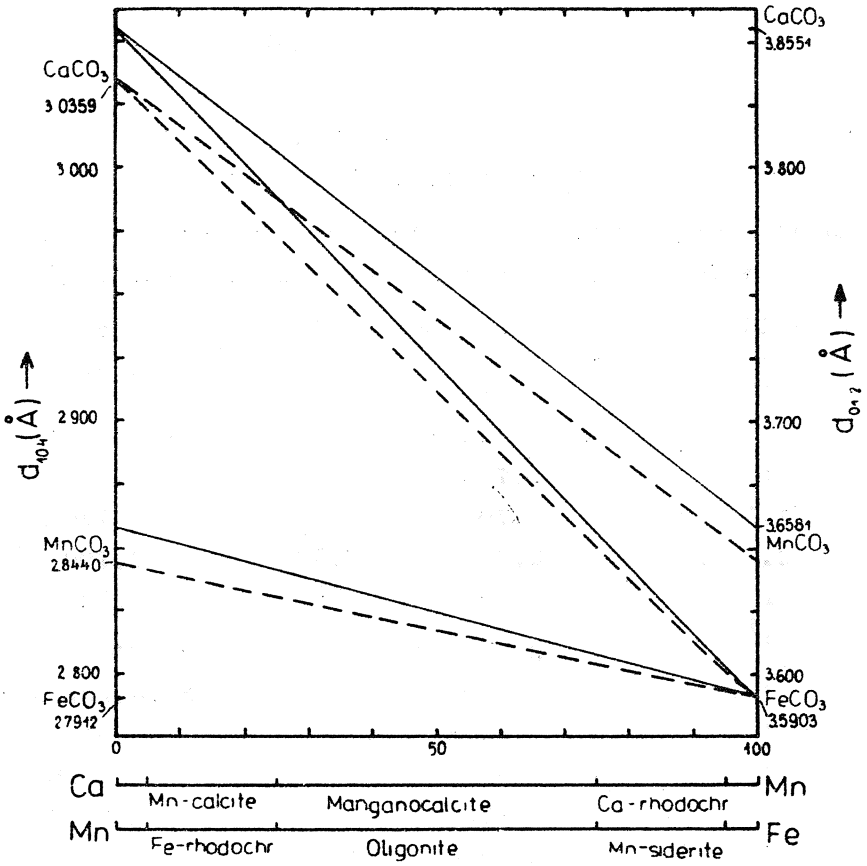

Fig. 6. Interplanar spacings versus rhombohedral carbonate composition (mol. percents) in the isomorphous series calcite-rhodochrosite, calcite-siderite and rhodochrosite-siderite. Solid and dashed lines denote $d_{01.2}$ and $d_{10.4}$ spacings, respectively. X-ray data after Graf (1961)

Fig. 6. Zależność odległości międzypłaszczyznowych od składu chemicznego romboedrycznych węglanów w szeregach izomorficznych: kalcyt-rodochrozyt, kalcyt-syderyt, i rodochrozyt-syderyt. Linie ciągłe i kreskowane wyznaczają zmienność odstępów $d_{01.2}$ i $d_{10.4}$, odpowiednio. Dane rentgenograficzne za Graf'em (1961)

In the first variety, represented by Harbutowice 30 sample, there occurs a small admixture of phosphate mineral (P_2O_5 — 2.72 wt. percent in the whole sample) not revealed by X-ray patterns. This sample is also noteworthy due to the appearance of two kinds of carbonate minerals — coarser grained and more frequent manganiferous siderite or oligonite and less abundant, finer grained calcareous siderite with overlapping X-ray lines ($d_{10.4}$ = 2.8047 Å and $d_{01.2}$ = 3.6074 Å, what corresponds to 27—25 percent $MnCO_3$ or 6.5 percent $CaCO_3$ molecule). Both carbonates, as well as, small amounts of additional pyrite could be distinguished in DTA curve (Fig. 5). Sub-to euhedral, rhombohedral grains of carbonate, with mean diameter = 0.1—0.2 mm, owe their automorphism to septechlorite matrix.

As could be expected, the carbonate-rich nodules, intermediate in

composition to their ferromanganese-oxide equivalents, are not infrequent. In this second variety, the undoubtedly secondary oxide minerals, like geothite and often pyrolusite, are the only alteration products. From numerous examples, the following are most characteristic: Działek 13, Lachowice 18 and Jastrzębia 19. Many of the remaining samples of nodules are provided with thin, oxide-bearing rims. The quantitative proportions between goethite and pyrolusite, naturally, vary with the composition of primary carbonate and diffusion ability of manganese compounds. It is well known, that manganese dioxide might be generated only under faintly alkaline conditions (in acid solutions Mn^{2+} does not oxidize into Mn^{4+}). The stratiform concretion, labelled as Działek 13 for the whole sample and 13b and 13c for crust and core, resp., is inhomogeneous in its composition. In the core, manganiferous siderite with nearly 10 percent of $MnCO_3$ ($d_{10.4}$ = 2.7947 Å) is accompanied by less abundant Ca-rhodochrosite ($d_{10.4}$ = 2.8172 Å), whereas the slightly goethitized peripheral part of concretion consists of carbonate of less defined (broad $d_{10.4}$ line near 2.80 Å) and rather widely varying composition between oligonite and Mn-siderite (see Fig. 2,10 and Fig. 4). The relics of not entirely replaced quartz sand grains, hydromuscovite flakes, glauconite granules and chloritized clay cement are still, everywhere, visible in microgranular (6—20 μm in ϕ), anhedral carbonate aggregate mass. In the curst (13b) excluding quartz, goethite is the only mineral discernible by X-ray techniques (Fig. 2,11).

The flattened nodule from Lachowice 18 is composed, both in peripheral and core part, of goethite, pyrolusite and siderite. Pyrolusite in highly dispersed form (see Fig. 4) must be considered as an alteration product of the manganese carbonate molecule of oligonite, while goethite resulted from incomplete iron carbonate transformation. The thin contractional veinlets of the nodule interior are built by quartz in detrital and reprecipitated generations. On the other side, in the immediate vicinity of concretion (18a), metasomatic processes of chloritization preceding carbonatization (oligonite ± calcite) may be deduced from microscopic examinations.

The Jastrzębia 19 mushroom cap-shaped concretion is in its internal, planar (bottom) part composed of goethite, pyrolusite and unaltered oligonite ($d_{10.4}$ = 2.8117 Å = 37 percent of $MnCO_3$), as well as, of rhodochrosite ($d_{10.4}$ = 2.8490 Å = some percent of additional $CaCO_3$ and (or $FeCO_3$). These two last minerals occur in almost equal quantitative proportions (Fig. 4). Numerous residual, primarilly detritic, hydromuscovite flakes are observed. In the peripheral, convex (top) part, goethite and ferroferous rhodochrosite ($d_{10.4}$ = 2.8406 Å = 5—6 percent $FeCO_3$) represent the only ferromanganese minerals.

From the almost unaltered carbonate nodules, those derived from Zembrzyce 16, Lgota 17, Bukowiec 20 and Ślemień 21 sites of occuren-

ce may be clearly subdivided into two varieties. The first (successively third) comprising the Zembrzyce 16 and Ślemień 21 samples contain Ca-rhodochrosite as index mineral, while the second (fourth) with Lgota 17 and Bukowiec 20 samples — oligonite and Mn-siderite.

Table - Tabela 1c

X-ray data of minerals of the ferromanganese-carbonate nodules: Cu K_α radiation, Ni filter

Dane rentgenograficzne minerałów konkrecji żelazisto-manganowo-węglanowych: promieniowanie Cu K_α, filtr Ni

Zembrzyce 16		Bukowiec 20		Ślemień 21	
d (Å)	I/I_o	d (Å)	I/I_o	d (Å)	I/I_o
Ca-rhodochrosite		Oligonite		Ca-rhodochrosite	
3.6811	2	3.6159	3	3.7026	2
2.8684	8	2.8053	9	2.8910	5 b
2.4032	1	2.3588	2	2.4076	1.5 b
2.1858	1	2.1395	2.5	2.1959	2 b
2.0097	1.5	1.9708	2.5	2.0224	2 b
1.8180	0.5[1]	1.8063	1	1.7941	2.5 b
1.784	4 b	1.7398	4	1.5481	0.5 b
1.5408	1[1]	1.5073	1.5	Oligonite	
Quartz		Quartz		2.8231	1
4.256	0.5	4.25	tr	Quartz	
3.343	4 a.o.	3.343	1	4.25	tr
Kaolinite				3.343	0.5
7.1	0.5 a.o.				

1 - coincidence of Ca-rhodochrosite with quartz, b - broad, tr - traces

The Ca-rhodochrosite nodules from Zembrzyce 16 and Ślemień 21 display peculiar ash-grey colour, ellipsoidal to discoidal shape, dense structure and conchoidal fracture. Microgranular (6—15 μm in diameter) aggregate of anhedral grains of Ca-rhodochrosite contains only small impurities in the form of quartz and hydromuscovite silt with illite (especially Ślemień 21, see Fig. 4) or kaolinite (Zembrzyce 16, see Table 1c) clay and bituminized and coalified plant remnants. The lattice spacings presented on Table 1c indicate calcium carbonate content ranging from 12 to 23 percent in Zembrzyce 16 and 24 to 34 percent in Ślemień 21, depending on the degree of Mn-Fe substitution. The cell parameters range from a = 4.799 Å, c = 15.672 Å, c/a = 0.327 in Ca-rhodochrosite with 12 percent $CaCO_3$, to a = 4.821 Å, c = 16.029 Å and c/a = 0.332 in Ca-rhodochrosite with 24 percent $CaCO_3$, repectively (see for interplanar spacings in Table 1c). Moreover, one of the Ślemień 21 samples reve-

aled the presence of small admixture of dolomite-ankerite with $d_{10.4}$ = 2.8897 Å and intensity four times lower than that of Ca-rhodochrosite.

The Mn-siderite and oligonite nodules (fourth variety) from Lgota 17 and Bukowiec 20, respectively, differ in some details. The former type exhibits layered form with brecciated structure and the last occurs as irregularly shaped, dense, crustified concretions and nests.

The manganiferous siderite samples (Lgota 17), except carbonate component, contain pyrite and Fe-septechlorite as essential minerals (see Fig. 4). The microgranular to fine-grained aggregate of Mn-siderite ($d_{10.4}$ = 2.7963 ≃ 10 percent $MnCO_3$, see Fig. 6) in some fragments is impregnated by late, intergranular Mn-siderite ($d_{10.4}$ = 2.7994 ≃ 18 percent $MnCo_3$), pyrite and Fe-septechlorite (replaced clay cement relics?). Pyrite grains also show the from of independent fragments which in some cases are half pyritized gaize-type sediments or subrounded, monomineralic, excluding small siderite veinlets (Plate I, Fig. 2). There is evidence of quartz sand replacement by carbonate, beginning from fissures, as well as, of the presence of late generation of Fe-septechlorite, filling pores.

The oligonite concretions or nests (Bukowiec 20) yield many examples of unaccomplished replacement of marly and silty sandstone by carbonate. They are evidently varying in composition, whereby carbonate grains in the internal parts (on the average 0.01 mm in diameter) contain 28 percent $MnCO_3$ ($d_{10.4}$ = 2.8053 Å, a = 4.730 Å, c = 15.402 Å, c/a = 0.315) and correspond to oligonite, while those of remaining parts (grain size — 0.03 mm) are built of Mn-siderite containing 20 percent $MnCO_3$ ($d_{10.4}$ = 2.8017 Å). As additional components diversely metasomatized quartz and glauconite, almost completely replaced feldspar and well preserved detritic hydromuscovite were observed. In the center of the concretion clay cement was transformed into Fe-septechlorite. In marginal part carbonate undergoes goethitization in varying degree.

CHEMISTRY OF NODULES

As may be deduced from the above presented considerations the nature and quantitative proportions of mineral components of nodules vary considerably, depending both on chemical composition of substratum + adsorbed material and on physico-chemical conditions under which its consolidation took place.

It is difficult now to envisage the chemistry of source material due to large-scale transformations during its long evolution. The only available indication provides the unreplaced, relict sediment in the form of sandstone or other porous and permeable material. Excluding metasomatic mode of growth of nodules, mechanic replacement by growing neo-

crysts and syn-depositional growth by accretion must be taken into account.

The silica content presents a notable criterion for quartz sand and siliceous organic detrite abundance, while alumina and lime might prove useful in evaluating clayey, marly or calcareous additions in the primary sediment. After carbon dioxide content it is not possible to establish the primary carbonate content, owing to the release of supplementary CO_2 by organic remnants decay and possible secondary carbonatization with rising partial pressure. The titanium dioxide, as chemically inert, appears in variable quantities depending rather upon the extent of leaching processes.

Many authors pointed out a distinct covariance between O/Mn and Mn/Fe ratios in recent ferromanganese nodules in respect to environmental conditions of their formation. This is especially true in the case of oxidation potentials, unfortunately significantly modified during diagenetic and post-diagenetic transformations of fossil nodules. Furthermore, the environment, as well as provenance features of nodules may be deduced from trace element absolute content and covariance, but the paucity of quantitative data precludes far reaching conclusions.

A. Hydrous ferromanganese-oxide nodules. Chemically, the first variety (Harbutowice 2) of this category of nodules distinguishes high O/Mn ratio = 1.84, which is due to secondary rather than original high oxidation state. Judging from the practical absence of titanium dioxide and small content of silica and alumina the growth by accretion or carbonate nature of original module may be implied. This conclusion is also in accordance with the scarcity of chromium, while abundance of copper supports accretional mode of formation as more justified.

The formerly postulated secondary nature of second variety (Lachowice 9 and 15) is evidenced by high O/Mn ratio = 1.87 and 2.00. The divergence in the silica and alumina content of sample no. 9 and 15, similarly to titania variability, is influenced by the chemistry of substratum rather then by the intensity of leaching processes. Supposed abnormal abundance of fine silt and clay, usually enriched in leucoxene, in the former (9) sample finds confirmation in the high content of silica, alumina and chromium. Increased barium and strontium contents (Table 5) in both samples should also be emphasized, as well as, the antagonistic behaviour of copper and nickel against zinc.

The low steric requirements of the third (no. 6), fourth (no. 7) and fifth (no. 23) variety (rich in „manganous manganite" mineral phases and accordingly showing rather low O/Mn ratio = 1,71 and 1.35) are insignificantly expressed by elevated minor and trace element contents. The undissolved relict, finely clastic, material is not uncommon, judging from SiO_2, Al_2O_3, TiO_2 and Cr quantitative data.

Table - Tabela 2a

Chemical analyses of major elements in the ferromanganese-oxide nodules/in weight percents of oxides/

Analizy chemiczne głównych pierwiastków w żelazistomanganowo-tlenkowych konkrecjach /w procentach wagowych tlenków/

Sample no.	SiO_2	TiO_2	MnO_2	Al_2O_3	Fe_2O_3	FeO	CaO	MgO	MnO	Na_2O	K_2O	Li_2O	H_2O^+	H_2O^-	CO_2	Total
2	6.43	-	33.70	1.66	42.15	-	0.30	1.19	5.07	0.10	0.31	0.08	7.32	1.78	-	100.09
6	14.10	0.35	15.80	6.60	45.12	-	0.22	2.02	5.21	0.16	0.54	0.11	8.03	1.17	-	99.43
7	18.32	0.40	25.28	7.99	25.09	-	0.73	0.84	8.87	0.33	0.46	n.d.	9.93	1.66	-	99.40
9	19.25	0.83	27.73	7.31	33.59	-	0.50	0.42	3.24	0.24	1.06	0.06	3.70	1.82	-	99.72
15	6.01	0.05	39.55	1.22	36.20	-	0.66	0.30	-	0.20	0.89	0.06	11.77	2.04	-	98.93
23	12.02	0.09	13.77	4.98	4.92	8.98	5.40	1.32	26.13	0.46	0.86	n.d.	3.15	1.30	16.43	99.81

Table - Tabela 2b

Chemical analyses of major elements in the phosphate-rich nodules/in weight percents of oxides/

Analizy chemiczne głównych pierwiastków w bogatych w fosforany konkrecjach/w procentach wagowych tlenków/

Sample no.	SiO_2	TiO_2	MnO_2	P_2O_5	Al_2O_3	Fe_2O_3	FeO	CaO	MgO	MnO	Na_2O	K_2O	H_2O^+	H_2O^-	CO_2	Total
22	10.61	-	3.01	7.06	7.25	2.11	13.64	9.97	0.59	20.45	tr.	0.06	2.81	0.88	22.01	100.50
25	26,26	-	-	12.87	22.61	4.58	11.05	12.00	0.12	0.53	tr.	0.15	1.54	0.22	8.03	99.96
28	34.26	-	-	13.97	21.62	2.71	-	17.20	0.02	2.40	tr.	0.30	3.32	0.32	4.32	100.44
29	12.72	0.13	19.91	8.21	1.29	3.10	5.91	11.91	0.21	10.47	tr.	0.05	8.62	1.27	16.52	100.32

22-F_2=0,19; 25-F_2=0,49; 28-F_2=0,52; 29-F_2=0.29 percent

Table - Tabela 2c

Chemical analyses of major elements in the carbonate Fe-Mn-rich nodules/in weight percents of oxides/

Analizy chemiczne głównych pierwiastków w bogatych w Fe i Mn konkrecjach węglanowych /w procentach wagowych tlenków/

Sample no.	SiO_2	TiO_2	MnO_2	Al_2O_3	Fe_2O_3	FeO	CaO	MgO	MnO	Na_2O	K_2O	Li_2O	H_2O^+	H_2O^-	CO_2	S	Total
13	19.25	0.16	-	5.50	19.62	12.00	4.23	1.03	12.56	0.29	0.91	0.11	3.52	0.92	19.59	-	99.69
13 b	31.97	0.28	5.50	7.52	16.79	13.95	0.83	0.91	-	n.d.	n.d.	n.d.	11.17	1.30	9.54	-	99.76
13 c	18.54	0.20	-	2.29	-	18.04	5.07	1.04	21.45	n.d.	n.d.	n.d.	2.82	0.78	29.51	-	99.74
16	19.94	0.21	1.55	3.86	-	4.93	5.16	0.27	33.99	0.21	0.37	n.d.	0.64	0.46	28.14	-	99.73
17	9.96	0.20	-	6.56	-	34.35	7.43	1.47	6.49	0.12	0.59	0.08	2.82	0.72	25.22	3.86	99.87
18	9.53	0.32	32.37	5.11	17.07	8.60	5.40	0.14	-	0.28	0.84	0.06	9.51	1.40	9.02	-	99.65
18 a	52.84	0.73	-	14.32	13.35	-	0.17	0.83	2.99	n.d.	n.d.	n.d.	12.05	1.35	-	-	98.63
18 b	11.12	0.39	20.90	6.56	14.02	8.72	4.98	0.04	3.97	n.d.	n.d.	n.d.	15.07	2.10	11.73	-	99.60
18 c	4.02	0.23	31.76	1.97	17.98	9.90	5.39	-	2.82	n.d.	n.d.	n.d.	11.15	2.35	11.97	-	99.54
19	10.96	0.28	14.50	6.47	26.63	5.57	4.75	0.35	9.64	0.13	0.58	n.d.	4.50	1.90	13.52	-	99.78
19 b	10.39	0.29	-	6.25	14.85	14.25	7.68	0.16	11.49	n.d.	n.d.	n.d.	10.03	1.85	21.86	-	99.10
19 c	8.92	0.27	10.30	4.72	12.30	17.22	9.20	0.30	8.82	n.d.	n.d.	n.d.	2.98	1.32	23.22	-	99.57
20	20.07	0.11	-	8.75	6.37	25.37	0.28	1.46	10.78	0.37	0.65	n.d.	0.59	2.48	22.21	-	99,49
21	8.24	0.14	-	4.49	3.02	10.75	8.47	1.29	28.16	0.25	0.51	n.d.	1.42	0.83	32.08	-	99.65
30	7.02	-	-	-	-	41.64	4.18	-	4.19	n.d.	n.d.	n.d.	0.22	0.11	40.02	-	100.10

30-P_2O_5=2.72 percent

Table - Tabela 3

Contents of minor elements in comparison with some major elements of the ferromanganese-oxide, phosphate-rich and carbonate Fe-Mn-rich nodules /in ppm and weight percents, resp./

Zawartości śladowych i niektórych głównych pierwiastków w żelazisto-manganowo-tlenkowych, bogatych w fosforany oraz węglany Fe i Mn konkrecjach /w g/t i procentach wag., odp./

Sample no.	Ni	Co	Cu	Zn	Cr	Fe	Mn	Fe/Mn	Al
2	55	21	2143	91	7	29.47	25.21	1.16	0.87
6	260	18	824	223	71	31.55	14.01	2.25	3.49
7	72	9	350	105	86	17.54	22.83	0.76	4.22
9	64	12	556	99	117	23.49	20.01	1.17	3.86
15	150	16	1370	10	25	25.31	24.98	1.01	0.64
23	109	70	1302	87	58	10.42	29.01	0.35	2.63
22	n.d.	9	766	45	n.d.	12.07	27.63	0.43	3.83
25	49	6	2221	118	40	11.78	0.40	29.45	10.37
28	66	11	1978	114	42	1.89	1.84	1.02	4.03
29	n.d.	8	n.d.	71	n.d.	6.72	20.60	0.32	0.68
13	135	37	1818	78	137	22.99	9.72	2.36	2.91
13 b	110	69	398	78	88	21.06	3.47	6.06	3.97
13 c	53	14	1820	18	128	14.02	16.61	0.84	1.21
16	87	14	503	10	88	3.83	27.29	0.14	2.04
17	128	52	1156	20	26	26.70	5.02	5.31	3.47
18	90	28	646	32	61	19.27	20.45	0.94	2.70
18 a	88	37	166	n.d.	361	10.37	2.31	0.59	7.58
18 b	71	15	598	n.d.	150	16.57	16.27	1.01	3.47
18 c	68	15	428	n.d.	98	20.26	22.24	0.91	1.04
19	55	39	1528	119	17	22.94	16.65	1.37	3.42
19 b	57	26	1432	226	29	21.45	8.93	2.40	3.30
19 c	63	12	690	100	91	21.98	13.35	1.64	2.49
20	46	35	1418	205	120	24.17	8.37	2.88	4.62
21	51	17	978	40	205	10.46	21.83	0.47	2.37

B. Phosphate-rich nodules. The divergence in the silica and alumina content observed in the carbonate-poor samples (Dąbrówka 25 and Tarnawa Górna 28) can be assigned to two factors: clastic mineral nature and high colloidal silica (now chalcedony) admixture in sample no. 28, co-precipitated with the phosphate mineral phase.

In the carbonate-rich variety (Dąbrówka 22 and Tarnawa Dolna 29), the silica and alumina content (occurring chiefly in the form of clastic minerals), is smaller at the cost of much higher carbonate mineral (rhodochrosite) content.

Table - Tabela 4

Correlation coefficients for elements in 20 ferromanganese /without phosphate-rich/ nodules

Współczynniki korelacji dla pierwiastków w 20 żelazisto-manganowych/bez fosforanowych/konkrecjach

	Fe	Mn	Ni	Co	Cu	Zn	Cr	Al
Fe	1	-0.17	0.21	-0.03	0.32	0.46	-0.34	-0.14
Mn		1	-0.14	-0.50	0.09	-0.36	-0.44	-0.65
Ni			1	0.02	-0.10	-0.69	-0.04	0.00
Co				1	0.11	0.00	-0.01	0.01
Cu					1	-0.12	-0.44	0.00
Zn						1	0.05	0.00
Cr							1	0.67
Al								1

Another conspicuous difference between carbonate-poor and carbonate-rich nodules is expressed by the abundance of trace elements. Copper and zinc are much more, most probably biogenetically, enriched in the former, while barium and strontium — in the last varieties. This assumption, as well as, a conclusion concerning the remaining elements is only an approximation, owing to the deficiency of analytical data.

Table - Tabela 5

Barium and strontium content in the ferromanganese nodules after spectrographic determinations

Zawartości baru i strontu w konkrecjach żelazistomanganowych na podstawie oznaczeń spektrograficznych

	Sample no.																	
Element	2	6	7	9	15	23	22	25	28	29	13	16	17	18	19	20	21	30
Ba.....	3	3	3	4	4	3	3	3	1	3	2	1	1	4	3	2	3	1
Sr.....	1	2	3	3	3	3	2	-	1	3	2	1	1	3	3	2	3	2

1 = 0.01-0.05; 2 = 0.05-0.1; 3 = 0.1-0.5; 4 = 0.5-1.0 percent

C. Ferromanganese-Carbonate nodules. The first variety of ferromanganese-carbonate nodules (Harbutowice 30) is exemplified by almost pure carbonate aggregate, except for the small admixture of silica, chiefly in the form of septechlorite and phospohoria not confirmed by the appearance of the rentgenographically detectable francolite. Trace elements were not determined, excluding barium and strontium occurring in negligible amounts.

The second variety (Działek 13, Lachowice 18 and Jastrzębia 19) exhibits pronounced differentiation in chemistry following mineral zonation in the growing and altering nodules. From core to the margin the clastic mineral contamination and Fe/Mn ratio increase, partly due to the greater mobility of Mn compounds, while O/Mn ratio remains variable. There is no regularity in the trace element distribution.

The variety characterized by unaltered Ca-rhodochrosite as the prevailing mineral (Zembrzyce 16 and Ślemień 21) and that consisting mainly of Mn-siderite or oligonite (Lgota 17 and Bukowiec 20) reveal no appreciable differences in major element composition. In trace elements spectra there is an evidence of enrichment in copper, cobalt and zinc in the third variety in respect to the fourth one.

All kinds of described nodules were also analyzed for bitumen A (extracted by chloroform) content. The results in weight percentages are as follows: 6 — 0.06, 13 — 0.11, 16 — 0.11, 17 — 0.14, 18 — 0.06, 19 — 0.11, 20 — 0.06 and 21 — 0.07.

DISCUSSION AND CONCLUSIONS

The most important task which almost all authors are attempting to resolve is the reconstruction of environmental conditions of formation of fossil and recent ferromanganese nodules. It has long been recognized that the chemistry of recent Fe-Mn nodules varies significantly with environmental conditions. In contrast to deep-sea nodules those generated in shallow water environments have attracted much less attention. Only in the last two decades this gap was in some extent reduced. However, Buchanan many years ago had reported in his work from 1891 (!) ferromanganese nodules from Scottish lochs, postulating some important conclusions. He pointed out, a.o., small cobalt and nickel contents and lower oxidation state of manganese in respect to deep-sea nodules (O/Mn = 1.6 and 1,95, resp.[2]). As follows from this short remark and from the conclusions presented by other authors, trace and minor elements concentration, the relation O/Mn, as well as, Fe/Mn ratio in recent nodules must be discussed here in detail as valid for fossil nodules too. The importance of the two last features is also significantly revealed by the specific mineral composition of recent and fossil nodules.

As stated by Price (1967) and other authors, deep-water or pelagic nodules are characteristically enriched in transition elements and lead in regard to shallow-water ones. Ferromanganese nodules from marginal areas of the Pacific Ocean, according to the mentioned author, dis-

[2] Results confirmed by Calvert and Price (1970), and other authors.

play similar minor or trace metal contents to those of shelf seas which are often by one or two orders of magnitude less abundant than corresponding contents of open oceanic forms. Present and other workers agree that higher concentrations of zinc in shallow-water environments are due to abundance of brown algae in biomass deposited. The interpretation of abnormal concentrations of trace elements in deep-sea water is different because of a great number of factors, which must be taken into consideration. These are as follows:

1. Small accretion rate of sediments. Rapid sedimentation hinders the generation of ferromanganese concretions, especially those of oxide type which must be in permanent contact with sea water, directly or indirectly. The accelerated burial of nodules should thus lead to partial removal, among others, of trace elements or even to their destruction.

2. Restricted mass of organic matter in sediments. The increased amount of organic matter lowers the oxidation ratio in sediments and favours fixation of iron (most effectively in the form of pyrite) and migration of manganese in manganous state.

3. The halmyrolitic decomposition of volcanic material, especially if of basaltic, hyaloclastitic nature, releases conspicuous amounts of trace elements. Submarine volcanic exhalations are often regarded as subordinate source. The alimentation by terrestrial sources should also be taken into account.

4. Concentration of trace elements by pore waters. As stated by numerous authors, the so-called pore or interstitial water of fresh bottom deposits of oceans contains much larger quantities of dissolved trace elements than does oceanic water. Anomalous amounts of manganese were released during bacterial decay of organic substances in the reduced manganous state of solvate, which after upward migration reprecipitated in higher oxidized states of oxides occuring in concretions. The same happens with iron, nickel and cobalt, but no evidence for a similar migration of zinc and copper is available (Addy et al., 1967). The decaying matter favours solution of transition metals and lead in the form of metal ions and metal chelates in true solution, not colloidally dispersed. The concentration gradient between pore and bottom waters, as well as, the pH, E_h differences between reduced and oxygenated environments create and maintain diffusion potential, causing upward migration.

5. The metal scavenging effect in highly oxidized manganese compounds, especially those displaying manganous manganite structure. Burns and Fuerstenau (1966) have shown that Ni, Cu, Zn, as well as Mg, K and Ba replace Mn^{2+} in this phase corresponding to todorokite a mineral common in deep-water concretions. Although the majority of cobalt occurs as absorbed by Fe^{3+} hydrated compounds, the nodules containing 10 Å manganite show lower Co content than nodules consist-

ing chiefly of 7 Å manganite and δ — MnO_2 (Burns and Fuerstenau, op. cit.). Calvert and Price (1970) remarked that in the Loch Fyne nodules Ba and Sr probably substitute for Ca and Mg, while divalent ions of Co, Mo, and Ni occur as replacing Mn^{2+} in the todorokite lattice. Another, less important scavenging effect is connected with adsorptive ability of Fe-Mn oxides, of clay minerals, of Al-hydroxide, and of silica, a.o. colloids or with the metabolism of organisms (Goldberg, 1954). Transition metal ions were found (Murray, 1975) to be adsorbed much more strongly on hydrous MnO_2 than alkaline earth metal ions. The observed order of adsorbability was as follows: Co $\geqq$ Mn $>$ Zn $>$ Ni $>$ $>$ Ba $>$ Sr $>$ Ca $>$ Mg. The selective and conspicuous concentration of some biophile microelements, like V, Mo, Ni, Co, Cu, Zn in selected varieties of planctonic or benthonic organisms is a commonplace phenomenon. After their death, the microelements, especially vanadium, were or were subsequently (during the diagenesis of sediments) fixed to some extent in complex metalloorganic compounds, e.g. non-migratory porphyrins, and in this way did not contribute to the enrichment of Fe-Mn nodules in trace elements.

The O/Mn and Fe/Mn ratios in ferromanganese concretions reflect oxidation potential conditions and in the second case also the quantitative proportions of both metal ions dissolved in pore waters. The oxidation potential value depends chiefly upon the organic matter abundance, the sulphur content in decaying organic matter, the rate of accretion of sediments and their permeability. The last factor allows more or less facilitated exchange between pore and bottom waters. The reduction of iron by sulphur compounds into insoluble iron sulphide and consequently into disulphide reduces iron content in pore water and, in consequence, the absolute value of Fe/Mn ratio in ferromanganese nodules. Simultaneously, judging from the diminished O/Mn ratio in near-shore concretions and high organic carbon content in host sediments, the rich biomass resulting from high supply of nutrients by neighbouring land influences (lowers) the oxidation state of manganese oxides (O/Mn = 1.6 in neritic and 1.95 in pelagic concretions). Seaward decrease of the organic carbon content in sediments, especially of humanic acids is not compensated by visible simultaneous augmentation of concentration of higher polymerised bitumens. In pelagic sediments these are, as a rule, saturated aromatic hydrocarbons, in contrary to unsaturated organic complexes in a neritic environment.

The variability of Fe/Mn ratio may also be explained by differences in the chemistry of substratum; basaltic rocks and their derivatives favour formation of Fe-rich concretions, while andesites — of Mn-rich ones. Some authors explain this phenomenon implying the activity of specialized Fe- or Mn-depositing Bacteria.

Another important indication helping to elucidate environmental con-

ditions of generation of certain ferromanganese nodules is their increased phosphate content. It has been already established that Late Cretaceous concretions and intercalations in the Carpathian Flysch deposits abound in phosphoria (Kamieński and Skoczylas-Ciszewska, 1955; Narębski, 1958, 1960; Jasionowicz et al., 1959). This is also true in respect to the studied rhodochrosite-francolite concretions of Lower Eocene and Mn-siderite or even francolite concretions of Middle Eocene or Palaeocene-Lower Eocene, respectively. The phosphate-rich nodules could not easily originate at shallow depth due to the biogenic (e.g. photosynthesis) impoverishement of waters and deposits in phosphorus, as well as at greater depth, where the supersaturation of the interstitial water in respect to solid francolite phase was hindered by increased partial pressure of carbon dioxide.

Analysing the bathymetric distribution of phosphate-rich water in the ocean and basin sediments, Bromley (1967) states that depths of over 300 m are unlikely to be suited for phosphorite formation. He also points out that the bulk of phosphate-phosphorus is released from descending organic matter before reaching the depth of 1000 m. However, in the restricted basins (trenches etc.) the sediments of turbidite origin may contain PO_4 — enriched interstitial waters and thus give rise to the generation of phosphate nodules even at great depth. The presence of diagenetic Fe-Mn carbonates and Fe-septechlorite emphasizes the moderate activity of oxygen during the formation of phosphate-rich nodules.

From the occurrence of layered rhodochrosite intercalations in the Eocene Variegated Shales (Książkiewicz, 1958) and in Cenomanian Radiolaria Shales, no significative bathymetric informations could be available for discussion. Such intercalations are known equally from shallow-water deposits (e.g. Baltic Sea, see Manheim, 1961), as well as, from deep-water sediments (trench off the coast of Chile, 5377 m depth, see Zen, 1959). It should be remarked that these layered intercalations, as well as, rhodochrosite concretions tend, always, to be genetically connected with finegrained sediments rich in organic matter. They are accumulated in the deeps, e.g. in the central, deepest parts of Loch Fyne (Calvert and Price, 1970), where overlying water is oxygen-poor or oxygen-free.

For reconstruction of environmental conditions of formation of fossil Fe-Mn nodules very important is the mineral composition of the host rock. A much restricted number of papers dealing with fossil ferromanganese nodules in world literature renders difficult the deduction of definite rules in this matter. However, in the majority of cases, the host rocks represent rather typical red-brown claystones, rich in Radiolaria and radiolarite intercalations or red „condensed" limestones. Formerly mentioned rocks, described by Molengraaff (1922) and Audley-Charles

(1965) from the Cretaceous and partly from the Jurassic and Triassic of East-Indian Archipelago do, in fact, closely resemble normal deep-sea clays. The „condensed" limestones of the Jurassic of Sicily have been formed, acc. to Jenkyns (1967) in an environment of minimal accretion of sediments in shallow-water on current-swept topographic highs. The ferromanganese nodules from both regions display peculiar concentric structure and composition resembling Recent deep-sea nodules.

The Carpathian Flysch sediments displaying features of deep-sea clays appear twice during the evolution of the external Carpathian geosyncline, namely in Cenomanian and in Palaeocene-Lower Eocene times. In both the cases their appearance can be connected with ocean floor spreading. This is expressed by the appearance of Radiolaria Shales rich in manganese and locally in clinoptilolite (Wieser, 1969, 1973). In the Palaeocene-Lower Eocene deposits of the Skole tectonic unit, brick-red to red-brown colour and very fine grain of shales present another striking features. It should be mentioned, that rhodochrosite intercalations have been observed in the Cenomanian and Eocene, while the Fe-Mn nodules corresponding to Recent deep-sea ones are known from Eocene deposits only.

Taking into account all the mentioned data, the following history of formation and subsequent evolution of the presently studied fossil ferromanganese nodules may be drawn (see also Fig. 7).

1. Ferromanganese-oxide nodules of compact texture and concentric structure (e.g. sample no. 7 and sample no. 23), containing the todorokite and birnessite as manganese minerals, originated in current-swept sediments of small accretion ratio and under rather free access of oxygen (Mn/O = 1.70—1.35). The host rocks of Lowest Eocene — Palaeocene or Lower Eocene age are enriched in manganese (compare low Fe/Mn ratio in nodules, equaling 0.76—0.35) and sometimes abound in clinoptilolite. This is the result of increased volcanic activity. Syn-sedimentary (syndepositional) accretion, but not replacement should here be implied, as a mode mechanism of concretionary growth.

2. Ferromanganese-oxide nodules with cellular structure (e.g. sample no. 9 and sample no. 15) are secondary after Fe-Mn carbonate nodules. They represent metasomatically originated carbonate nodules which by epigenetic and probably even hypergenetic processes have been transformed to hydrated and highly oxidized (Mn/O = 1.87—2.00) forms. Pyrolusite and hematite + goethite are key minerals, quantitatively appearing in similar proportions (Fe/Mn = 1.17 — 1.01). As their coeval equivalents, only partially oxidized may serve siderite (formerly oligonite) nodules with goethite and pyrolusite encrustations (sample no. 18).

3. Phosphate-rich carbonate nodules form all possible transitions to pure carbonate, ferromanganese nodules. Both are the products of dis- and replacement of sediments in their early diagenetic stage of lithifi-

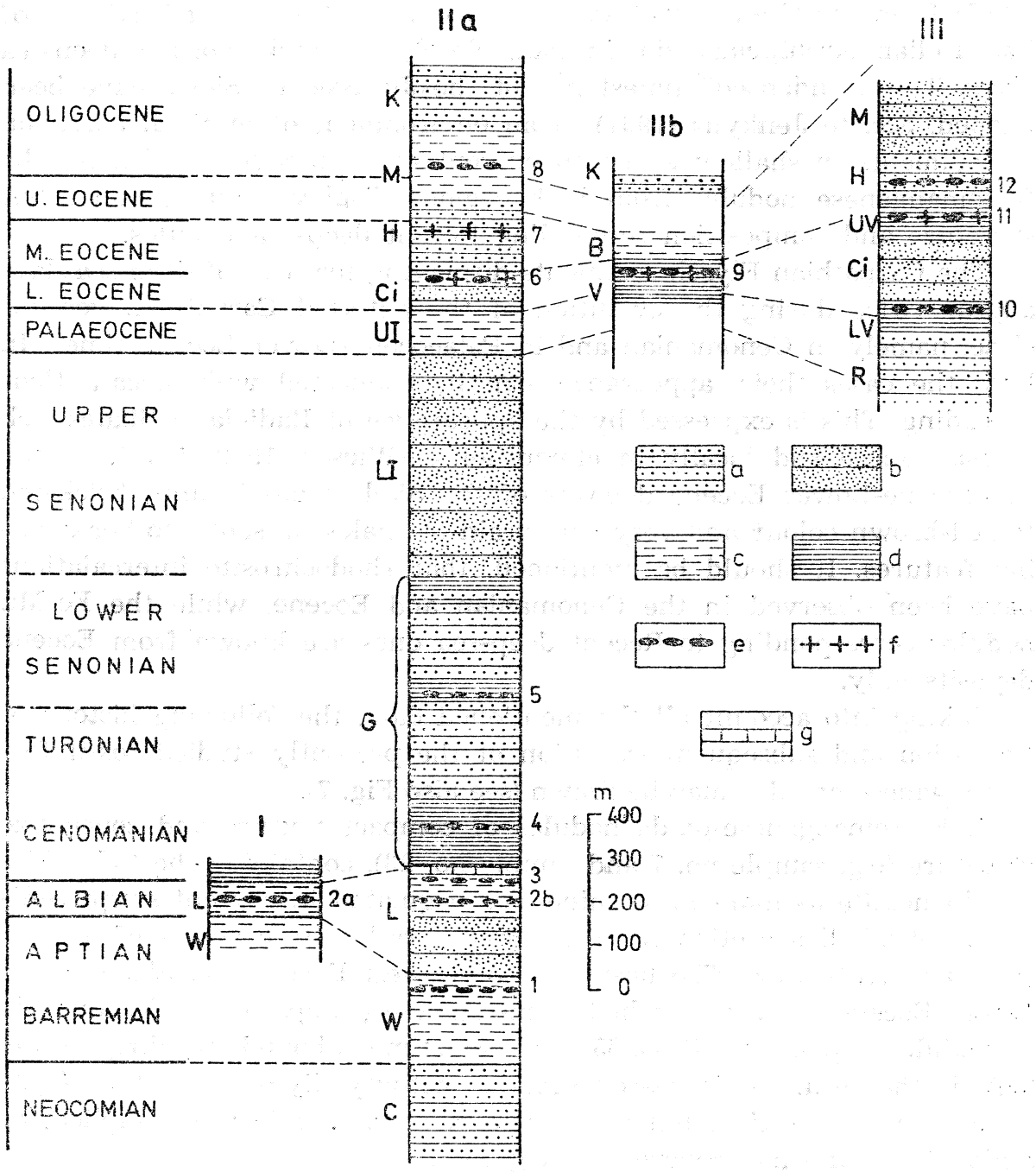

Fig. 7. Vertical distribution of ferromanganese and phosphate-rich concretions in the flysch of the Polish Western Carpathians (diagram prepared by M. Książkiewicz). I — Sub-Silesian nappe; IIa — Silesian nappe, Mały Beskid and Lanckorona zones; IIb — Tarnawa Górna — Śleszowice anticline; III — Magura nappe. a — thin-bedded flysch; b — thick- bedded flysch; c — black and dark shales; d — variegated (red and green) shales; e — ferromanganese concretions; f — phosphate--rich concretions; g — hornstones. C — Upper Cieszyn Shales; W — Veřovice Shales; L — Lgota Beds and their equivalents; G — Godula Beds; LI — Lower Istebna Beds; UI — Upper Istebna Beds; Ci — Ciężkowice Sandstone; H — Hieroglyphic Beds; B — black shales of Tarnawa Górna; V — Variegated Shales; M — Menilite Shales; K — Krosno Beds; R — Ropianka Beds; LV — Lower Variegated Shales; UV — Upper Variegated Shales; M — Magura Sandstone. Occurrences of concretions. 1 — Lgota; 2 — Harbutowice; 3 — Lanckorona; 4 — Jastrzębia; 5 — Bukowiec Mt., Rudnik; 6 — Dąbrówka, (in similar situation Ostrósza); 7 — Zembrzyce; 8 — Działek Mt., Stronie; 9 — Tarnawa Górna; 10 — Lachowice; 11 — Tarnawa Dolna; 12 — Ślemień

cation. Quartz and feldspar grains are easily replaced by carbonates and phosphates, while clayey cement normally is initially transformed to Fe-septechlorite, and then to carbonates and phosphates. The most reaction-resistant are detrital white mica flakes. Iron, manganese and phosphorus were supplied from the outside through interstitial water whereas calcium and magnesium were predominantly derived from the replaced material. This is in good accordance with the observed occurrence of Ca-rhodochrosite-bearing nodules in calcium carbonate-rich host rocks.

4. The most frequent kind of nodules in the Carpathian Flysch — the ferromanganese-carbonate nodules, commonly show mixed composition with distinct zonation. This is well expressed in the occurrence in the interiors of nodules of e.g., manganiferous siderite and/or Ca-rhodochrosite, and in peripheries — of oligonite or siderite with the secondarilly unmixed rhodochrosite molecule oxidized into Mn-oxides. This relation should be attributed to the greater mobility of iron and especially of manganese in freshly buried sediment under a high partial pressure of carbon dioxide in regard to calcium and magnesium. Copper, nickel, cobalt and phosphorus displayed a higher mobility, equal to manganese but higher than iron. Quite low mobility of vanadium and zinc was partly caused by the stability of metalloorganic compounds of these elements. Titanium and chromium should be treated as almost completely inert. Rather poor quantitative representation of the recorded trace elements in all types of nodules may be interpreted by the distant localization of volcanic eruption centers, which diminished the influence of volcanic exhalations and the content of easily decomposing glassy material in sediments. There is no significant correlation between major, minor and trace elements, excluding Al/Cr and inconspicuous Fe/Cu interdependence.

5. The pronounced variability of the chemical and mineral composition of the nodules with age, depends on the development of tectonic

Fig. 7. Pionowe rozmieszczenie występowań konkrecji żelazomanganowych i wzbogaconych w fosforany we fliszu polskich Karpat Zachodnich (diagram sporządzony przez M. Książkiewicza). I — płaszczowina podśląska; IIa — płaszczowina śląska, strefa Beskidu Małego i Pogórza Lanckorońskiego; IIb — płaszczowina śląska, siodło Tarnawa Górna — Śleszowice; III — płaszczowina magurska. a — flisz cienkoławicowy; b — flisz gruboławicowy; c — czarne lub ciemne łupki; d — pstre (czerwone i zielone) łupki; e — występowania konkrecji żelazomanganowych; f — występowania konkrecji bogatych w fosforany; g — rogowce. C — łupki cieszyńskie górne; W — łupki wierzowskie; L — warstwy lgockie i ich równoważniki; G — warstwy godulskie; LI — dolne warstwy istebniańskie; UI — górne warstwy istebniańskie; Ci — piaskowiec ciężkowicki; H — warstwy hieroglifowe; B — czarne łupki z Tarnawy Górnej; V — łupki pstre; M — łupki menilitowe; K — warstwy krośnieńskie; R — warstwy ropianieckie; LV — dolne pstre łupki; UV — górne pstre łupki; M — piaskowiec magurski. Stanowiska konkrecji: 1 — Lgota; 2 — Harbutowice; 3 — Lanckorona; 4 — Jastrzębia; 5 — góra Bukowiec, Rudnik; 6 — Dąbrówka (w podobnej sytuacji występują konkrecje w Ostrószy); 7 — Zembrzyce; 8 — góra Działek w Stroniu; 9 — Tarnawa Górna; 10 — Lachowice; 11 — Tarnawa Dolna; 12 — Ślemień

events in the outer Carpathian geosyncline. In the first stage of the geotectonic cycle, characterized by sediments of euxinic type of black or dark sediments, originated Mn-siderite nodules with Fe-septechlorite or even pyrite, indicating, a rather high reduction potential of the environment. The sample (no. 17) from Veřovice Beds (Barremian-Aptian) corresponds to siderite and sideroplesite concretions, as reported by Narębski (1957) from Upper Teschen Shales and Veřovice Beds, though being Mn-richer and Mg-poorer.

In the following stage, differing by the formation of slightly better aerated sediments (judging just from green colour of shales) secondarilly oxidized and hydrated goethite + pyrolusite concretions (e.g. sample no. 2), appeared in Lgota Beds, e.g. in Harbutowice (Lower or Middle Albian, pers. com. of dr J. Liszka). Similar bulk composition ranging from rhodochrosite to oligonite with secondary encrustations of pyrolusite and goethite distinguishes sample no. 19 from Lower Godula Beds (Cenomanian-Turonian). Noteworthy is the appearance of somewhat older (Cenomanian), so-called „Manganiferous Shales" in the Carpathian Flysch, containing unoxidized or oxidized rhodochrosite intercalations in associations with bentonites, clinoptilolite-bearing Radiolaria Shales and silica-rich sediments. These deposits beginning the sedimentation of the Variegated Shales with prevailing red colour are genetically in close relationship with volcanic and tectonic phenomena, which could be connected with the ocean floor spreading of the Thetis.

Also exhibiting oligonite composition is a concretion (sample no. 20) from Upper Godula Beds (Lower Senonian), while concretions described by Narębski (1957) from younger Upper Istebna Beds (Danian-Palaeocene) are of sideroplesitic or sideritic nature.

In Palaeocene-Lowest Eocene time another important tectonic event took place. The rejuvenation of the geosyncline connected with the ocean floor spreading of the Thetis initiated and accelerated the volcanic activity. The relicts of decomposition products of volcanites and products of volcanic exhalations are included in sediments which locally (especially in the Skole tectonic unit) display all the features of deep-sea clays (brick-red colour, high content of manganese, clinoptilolite as essential constituent, dolomite-ankerite a.o. microconcretions, etc.. Wieser, 1969). As might be expected, the chemistry of the nodules tends to demonstrate greater concentrations of manganese, phosphorus and fluorine. The first element abounds in goethite + todorokite or birnessite (e.g. samples nos 7 and 23) nodules and goethite + hematite + pyrolusite (after oligonite, samples nos 9 and 15) nodules. Phosphorus and fluorine, naturally, concentrate in rhodochrosite + francolite (samples nos 22, 29) and francolite (sample no. 28) nodules. Though some of these nodules are considered to belong to upper part of Lower Eocene (after Książkiewicz's age evaluation given to all samples), the most important is the evidence of

similar environmental conditions and a common source of elements in the Silesian and Magura sedimentary basins (and nappes).

In the Lower Hieroglyphic Beds and in the Upper Variegated Shales of the Lower-Middle Eocene, Ca-rhodochrosite and Mn-siderite + francolite nodules (samples, nos 16 and 21 or 25 and 29, resp.) seem to be just as typical as they are for Menilite Shales from the Eo-Oligocene (e.g. sample no. 13). As formerly emphasized, the presence of Ca-rhodochrosite is in genetic relation with the calcium carbonate content of substratum.

Further shallowing of basins (filled with $CaCO_3$-rich sediments) in the period of sedimentation of the Menilite-Krosno Beds lead to the formation of ankerite-dolomite concretions, studied by Narębski (1957).

Concluding, the followning general remarks should be emphasized:

1-o. The described goethite + todorokite ± birnessite associations have their equivalents in the ferromanganese nodules from ocean's and fjord's (deepest parts) bottom, as well as, in older fossil concretions. Carbonate and phosphate-rich Fe-Mn nodules, more typical for shelf seas could also originate in deep-water environment (Zen, 1959, a.o.).

2-o. The primary nodules of hydrated Fe-Mn oxide composition are the products of accretional growth, with material supplied by bottom and pore waters. The growth of carbonate and phosphate-rich Fe-Mn nodules depends completely upon the high concentration and diffusion gradients of pore waters and the dis- and replacement phenomena. Carbonatization of coarsely grained material (quartz, feldspars) was preceded by the septechlorite substitution of clay minerals, or less significantly, by pyritization.

3-o. The culmination of ferromanganese nodule abundance in the Carpathian Flysch deposits of Poland appears in the Eocene, shortly after the rejuvenation in Palaeocene-Lowest Eocene time of the external Carpathian geosyncline. The Albian and Cenomanian should be mentioned as another but less prominent epoch of ferromanganese nodule generation. In both cases, there is a good genetical accordance with the appearance of clinoptilolite-rich, Radiolaria shales.

Acknowledgments

The authors would like to thank graciously Prof. M. Książkiewicz of Jagellonian University, for stimulating this work and making available the samples used in this study, as well as, for providing maps, profiles and other informations concerning their stratigraphical and tectonic position. The authors are also grateful to ing. J. Stępiński from Institute of Metallurgy, Academy of Mining and Metallurgy, Kraków, for performing electron microprobe X-ray scans and scanning electron micrographs. We are also indebted to mgr H. Grabowski and ing. E. Ratajski for making micrographs and photographs of polished sections.

Manuscript received December 1977
accepted February 1978

REFERENCES — WYKAZ LITERATURY

Addy S. K., Presley B. J., Ewing M. (1976), Distribution of manganese, iron and other trace elements in a core from the Northwest Atlantic. *J. Sed. Petrol.* 46, p. 813—818, Tulsa, Oklahoma.

Audley-Charles M. G. (1965), A geochemical study of Cretaceous ferromanganiferous sedimentary rocks from Timor. *Geoch. Cosmoch. Acta* 29, p. 1153—1173, Oxford.

Bromley R. G. (1967), Marine phosphorites as depth indicators. *Marine Geology*, 5, p. 503—509, Amsterdam.

Brasseur H. (1950), Méthode permettant d'obtenir avec rapidité et précision le rapport c/a d'une apatite. *Acad. Roy. de Belg. Bull., Cl. d. Sci.* 36, p. 521—524, Bruxelles.

Buchanan J. V. (1891), On the composition of oceanic and littoral manganese nodules. *Trans. Roy. Soc. Edinburgh* 36, p. 459—484, Edinburgh.

Burns R. G., Fuerstenau D. W. (1966), Electron-probe determination of inter-element relationships in manganese nodules. *Amer. Min.* 51, p. 895—902, Menasha, Wisconsin.

Calvert S. E., Price N. B. (1970), Composition of manganese nodules and manganese carbonates from Loch Fyne, Scotland. *Contr. Min Petrol.* 29, p. 215—233, Stuttgart.

Frondel C., Marvin U. B., Ito J. (1960), New occurrence of todorokite. *Amer. Min.* 45, p. 1167—1173, Menasha, Wisconsin.

Goldberg E. D. (1954), Marine geochemistry. 1. Chemical scavengers of the sea. *J. Geol.* 62, p. 249—265, Urbana, Illinois.

Graf D. L. (1961), Crystallographic tables for the rhombohedral carbonates. *Amer. Min.* 46, p. 1283—1316, Menasha, Wisconsin.

Jasionowicz J., Koszarski L., Szymakowska F. (1959), Geologiczne warunki występowania konkrecji fosforytowych w pstrych marglach węglowieckich (górna kreda) Karpat Środkowych (Geological Conditions of Occurrence of Phosphoritic Concretions in the Węglówka variegated Marls (Upper Cretaceous) of the Middle Carpathians). *Kwart. geol.* 3, 4, p. 1016—1023, Warszawa.

Jenkyns H. C. (1967), Fossil Manganese Nodules from Sicily. *Nature* 216, p. 673—674, London.

Jones L. H. P., Milne A. A. (1956), Birnessite, a new manganese mineral from Aberdeenshire, *Scotland. Min. Mag.* 235, p. 283—288, London.

Kamieński M., Skoczylas-Ciszewska K. (1955), O skale wzbogaconej w P_2O_5 w Karpatach fliszowych. *Arch. Min.* 19, 2, p. 161—174, Warszawa.

Książkiewicz M. (1958), Stratygrafia serii magurskiej w Beskidzie Średnim (Stratigraphy of the Magura Series in the Średni Beskid (Carpathians)). *Inst. Geol. Biul.* 135, p. 43—95, Warszawa.

Kulp J. L., Perfetti J. N. (1950), Thermal study of some manganese oxide minerals. *Min. Mag.* 210, p. 239—251, London.

Ljunggren P. (1960), Todorokite and pyrolusite from Vermlands Taberg, *Amer. Min.* 45, 1—2, p. 235—238, Menasha, Wisconsin.

Manheim F. T. (1961), A geochemical profile in the Baltic Sea. *Geoch. Cosmoch. Acta*, 25, p. 52—70, Oxford.

Molengraaff G. A. F. (1922), On the Manganese Nodules in Mesozoic Deep-Sea Deposits of Dutch Timor. *Proc. Sect. Sci. Roy. Ac. Sci.* 23, p. 997—1012, Amsterdam.

Murray J. W. (1975), The interaction of metal ions at manganese dioxide-solution interface. *Geoch. Cosmoch. Acta* 39, p. 505—519, Amsterdam.

Narębski W. (1956), O diagenetycznych dolomitach żelazistych z Karpat fliszowych (with Russian summary). *Rocz. Pol. Tow. Geol.* 26, 1, p. 29—50, Kraków.

Narębski W. (1957), Mineralogia i geochemiczne warunki genezy tzw. syderytów fliszu karpackiego (Mineralogy nad geochemical conditions of formation of so-called siderites of the Carpathian Flysch). *Arch. Min.* 21, 1, p. 5—100, Warszawa.

Narębski W. (1958), Konkrecje fosforytowe z Wysokiej Strzyżowskiej (Karpaty Fliszowe) (Phosphorite concretions in Wysoka Strzyżowska (Flysch Carpathians)). *Pr. Muzeum Ziemi* 1, p. 165—170, Warszawa.

Narębski W. (1960), Konkrecje fosforytowe z pstrych margli węglowieckich (Karpaty fliszowe) (Phosphorite concretions of the Węglówka variegated marls Carpathian Flysch)). *Acta geol. pol.* 10, 2, p. 165—200, Warszawa.

Price N. B. (1967), Some geochemical observations on manganese-iron oxide nodules from different depth environments. *Marine geology* 5, p. 511—538, Amsterdam.

Straczek, J. A., Horen A., Ross M., Warshaw C. M. (1960), Studies of the manganese oxides. IV. Todorokite. *Amer. Min.* 45, p. 1174—1184, Menasha, Wisconsin.

Wieser T. (1969), Clinoptilolite from the Lower Eocene Variegated Shales of the External Flysch Carpathians. *Bull. Acad. Pol. Sci. Sér. sci géol. et géogr.* 17, 2, p. 123—129, Varsovie.

Wieser T. (1973), Klinoptylolit w łupkach radiolariowych cenomanu z Międzybrodzia, k. Sanoka. *Kwart. geol.* 17, 3, p. 651—652, Warszawa.

Zen E-An (1959), Mineralogy and petrography of marine bottom samples of the coast of Peru and Chile. *J. Sed. Petrol.* 29, p. 513—539, Tulsa, Oklahoma.

STRESZCZENIE

Zbadane konkrecje żelazomanganowe z osadów fliszowych Karpat Polskich zostały sklasyfikowane chemicznie w następujących trzech grupach: 1 — uwodnione, tlenkowe, 2 — węglanowe i 3 — bogate w fosforany (fig. 1—7, tabele 1—5, pl. 1—4).

Pod względem mineralogicznym do pierwszej z grup należą konkrecje o składzie: goethyt + todorokit ± birnessyt, ze zbitą koncentrycznie zonalną budową oraz goethyt ± piroluzyt ± hematyt, o charakterystycznej budowie komórkowej, zbitej i pręcikowej. Drugą grupę znamionuje występowanie, razem lub oddzielnie, oligonitu i Ca-rodochrozytu, podczas gdy trzecią grupę wyróżnia niemal monomineralny — frankolitowy lub mieszany — frankolitowo-rodochrozytowy skład.

Konkrecje złożone z goethytu, todorokitu ± birnessyt w pełni odpowiadają konkrecjom żelazowo-manganowym z dna oceanów i głębin fiordów oraz starszym konkrecjom kopalnym, opisanym zaledwie w kilku publikacjach. Konkrecje węglanowe i fosforanowe, bardziej typowe dla mórz szelfowych, mogły także powstawać i w warunkach głębokomorskich (Zen, 1959). Pierwotnie tlenkowe konkrecje żelazomanganowe narastały czerpiąc materiał wprost z wody morskiej i z wód porowych, natomiast węglanowe i fosforanowe — wyłącznie z wód porowych, roztwo-

rów o wysokim gradiencie koncentracyjnym i dyfuzyjnym. W ostatnim przypadku dużą rolę odegrały także i procesy metasomatyczne, jak poprzedzające karbonatyzację kwarcu, skaleni i in. zastąpienie minerałów ilastych przez septechloryty czy rzadsza pirytyzacja. Najodporniejsze dla tych procesów zastępowania były grubiej okruchowe jasne miki.

Maksimum nagromadzenia konkrecji żelazomanganowych w osadach fliszowych Karpat Polski obserwuje się w eocenie, tj. po przypadającej na granicę paleocenu i eocenu rejuwenacji geosynkliny zewnętrznych Karpat. W tym to okresie osadzały się w skolskim basenie sedymentacyjnym głębokomorskie, radiolariowe, ceglasto-czerwono-brunatne, bardzo drobnoziarniste iłowce z klinoptylolitem i swoistymi kryształami i mikrokonkrecjami węglanowymi (Wieser, 1969). Podobne zjawiska tektoniczne połączone z „oceanizacją dna" i ze wzmożoną aktywnością wulkaniczną miały miejsce w albie i cenomanie. Z cenomanu znane są lokalnie bardzo bogate w klinoptylolit iłowce radiolariowe.

W opracowanych konkrecjach nie zauważono podwyższonej zawartości pierwiastków śladowych, jak również wyraźnej korelacji między pierwiastkami głównymi, pobocznymi i śladowymi. Wyjątek stanowi korelacja między glinem i chromem, zawartych głównie w minerałach ilastych oraz mniej dostrzegalna korelacja między żelazem i miedzią. Stosunkowe ubóstwo pierwiastków śladowych najlepiej tłumaczy znaczna odległość od centrów aktywności wulkanicznej.

EXPLANATIONS OF PLATES — OBJAŚNIENIA PLANSZ

PLATE — PLANSZA I

Fif. 1. Manganiferous siderite (Mn = 2.2 weight percent) nodule, co-occurring with ferromanganese-oxide one (Harbutowice 4 and 2, resp.). The visible metasomatic veinlet with prevailing hydrous Fe-Mn oxides (goethite the only detectable by X-ray techniques mineral constituent) follows contractional fracture. The alteration proceeds outwards from this fracture. Thin section, × 10

Fig. 1. Konkrecja manganonośnego syderytu (Mn = 2,2% wag.), współwystępująca z konkrecją żelazomanganowo-tlenkową (Harbutowice 4 i 2, odp.). Widoczna żyłka metasomatyczna z przeważającymi wodnymi tlenkami Fe-Mn (goethyt jako jedyny składnik wykrywalny metodami rentgenograficznymi) wiąże się ze szczeliną kontrakcyjną. Przeobrażenie przebiega na zewnątrz od tej szczeliny. Płytka cienka, × 10

Fig. 2. Brecciated structure of manganiferous siderite intercalation. Numerous subrounded and fine-grained pyrite aggregate fragments are cut by siderite veinlets. Lgota 17. Thin section, × 10

Fig. 2. Tekstura brekcjowa wkładki syderytu manganonośnego. Liczne półobtoczone fragmenty drobnoziarnistego agregatu pirytowego poprzecinane żyłkami syderytowymi. Lgota 17. Płytka cienka, × 10

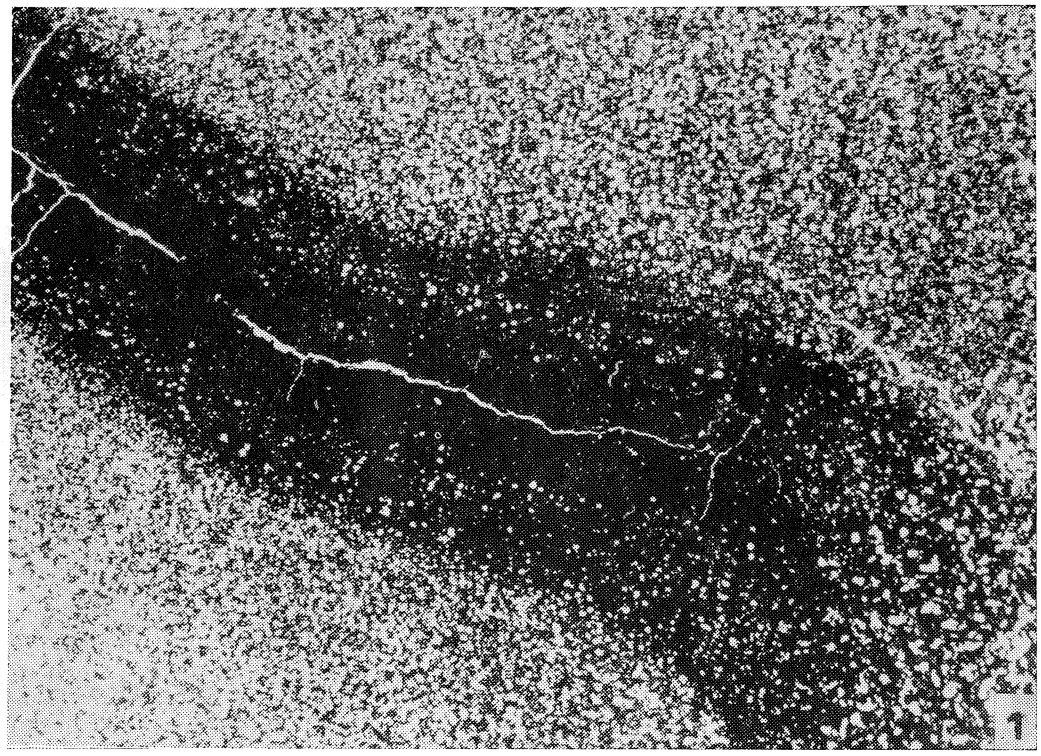

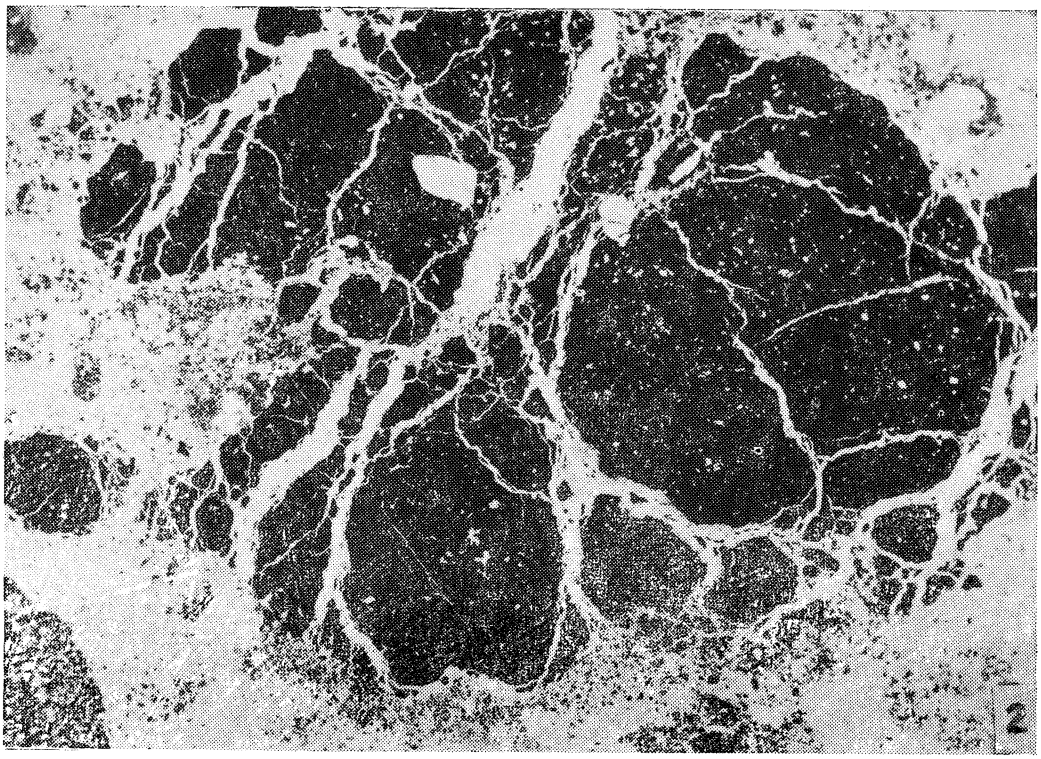

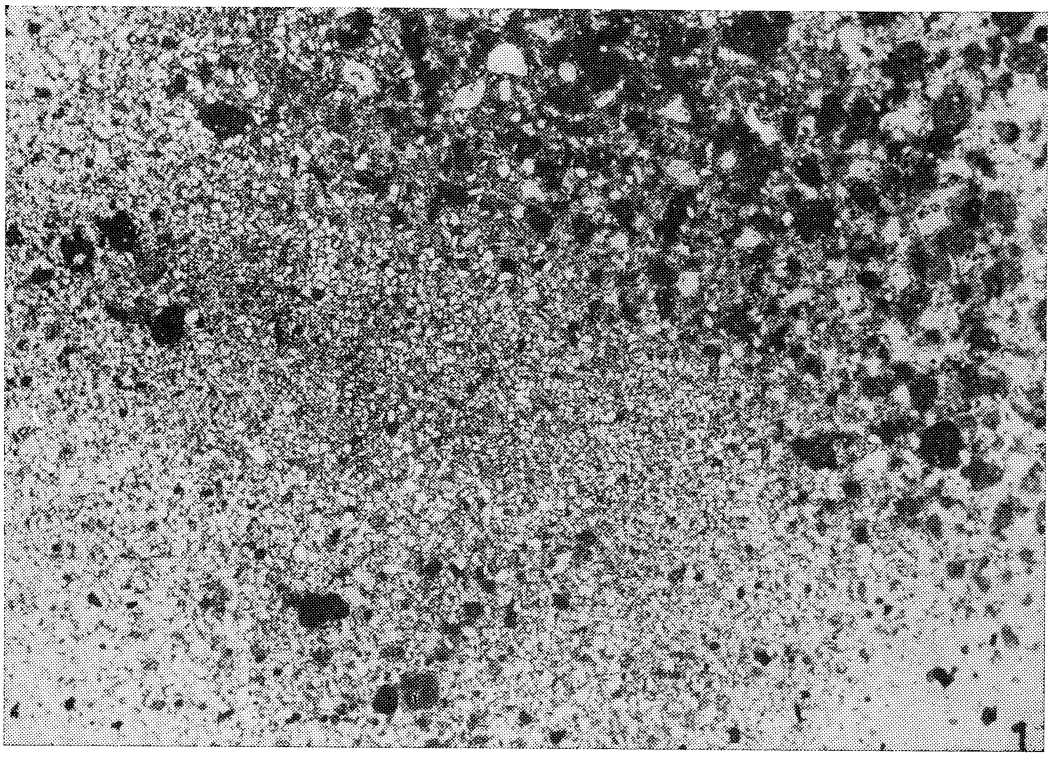

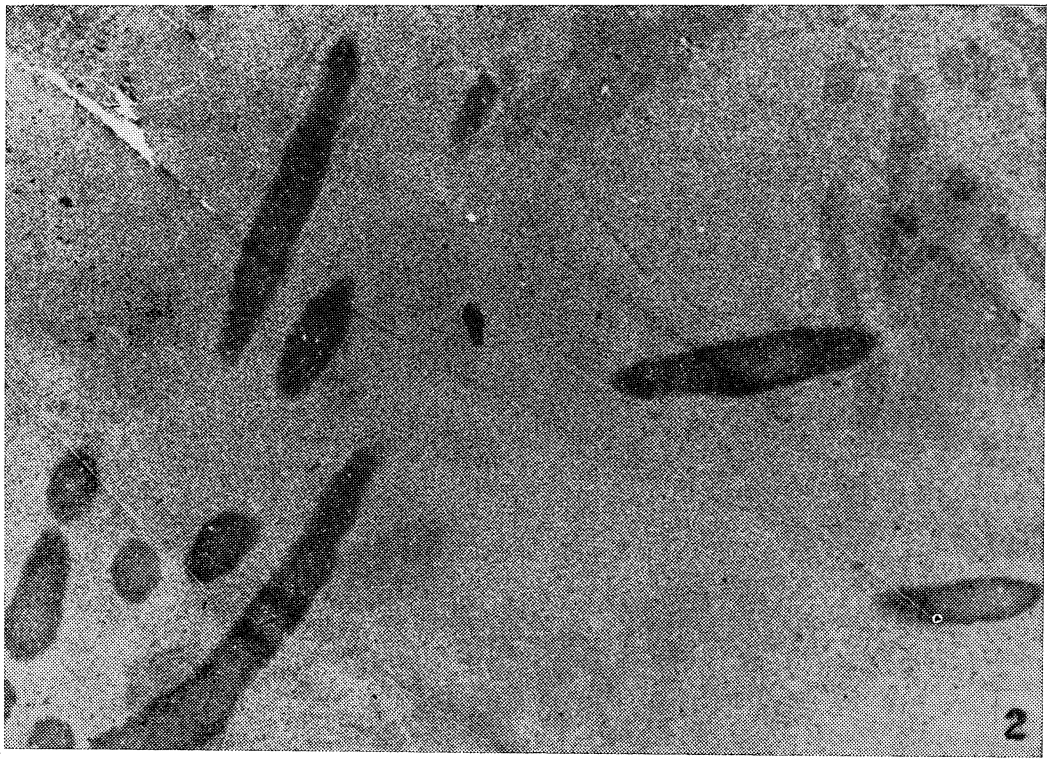

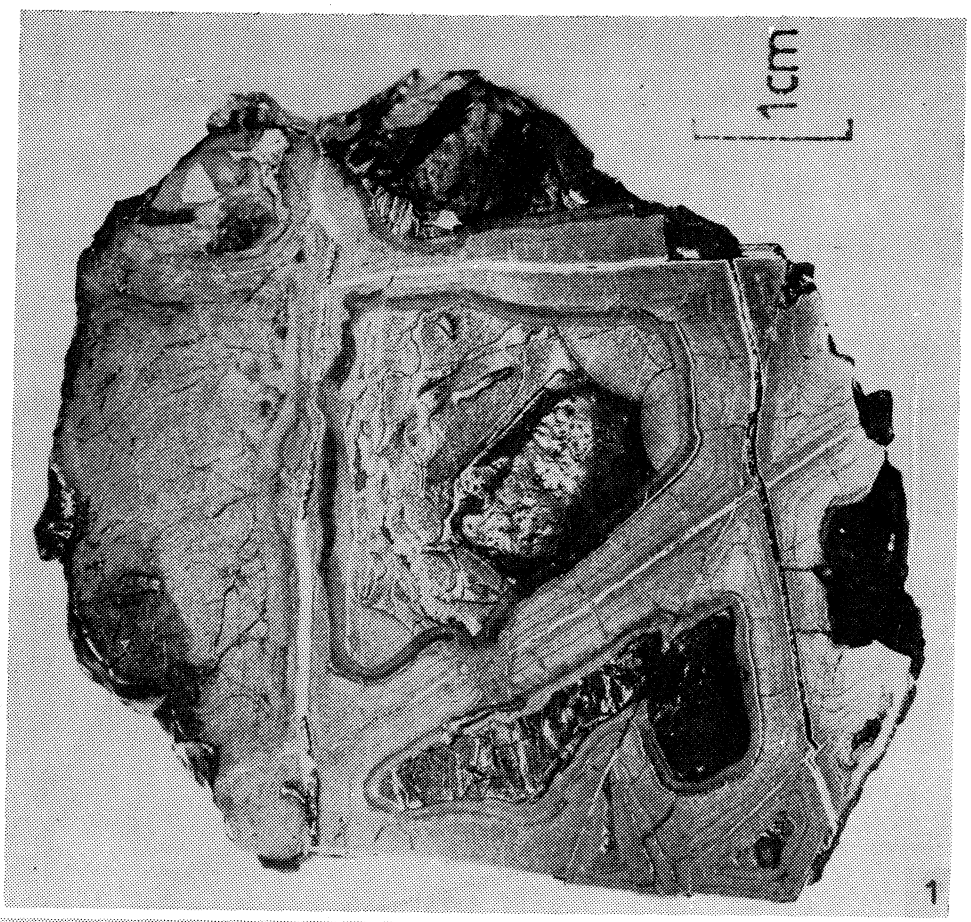
1 cm
1

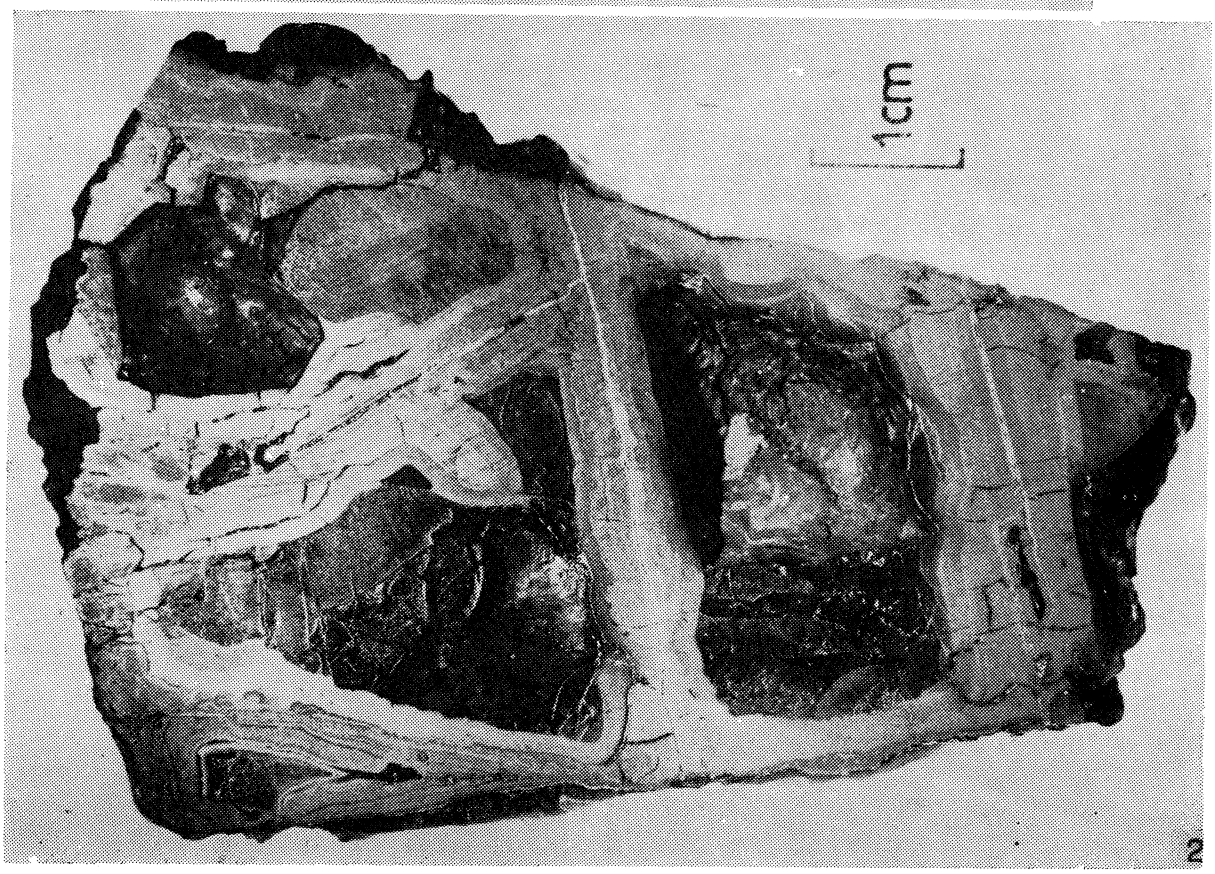
1 cm
2

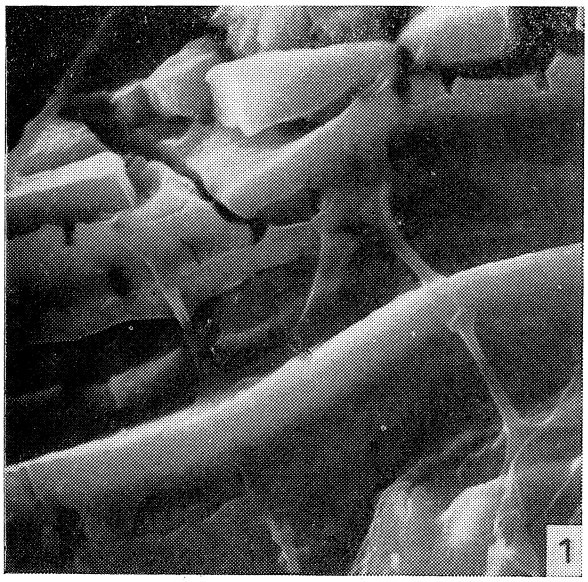
1

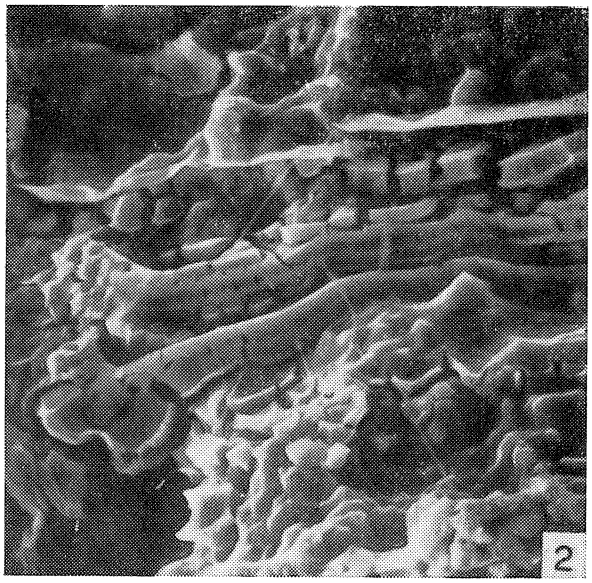
2

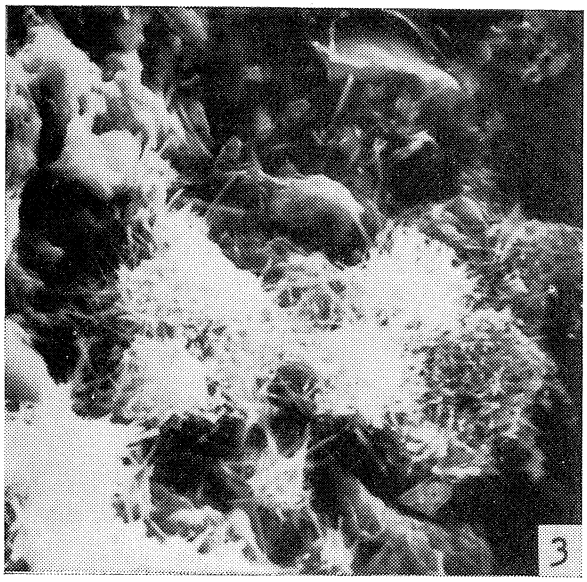
3


4

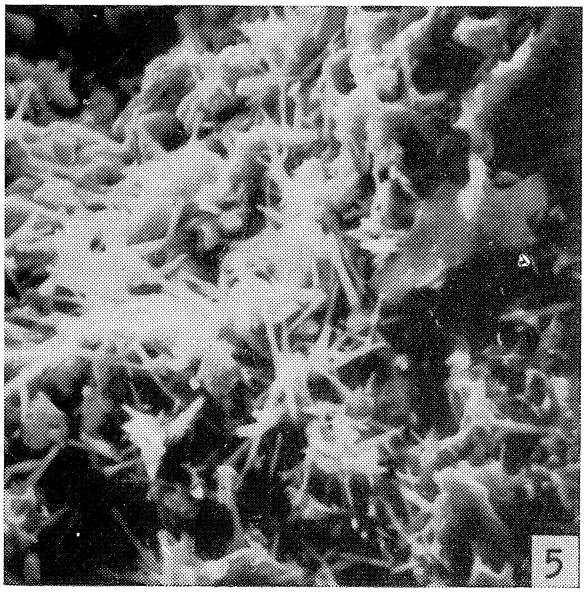
5

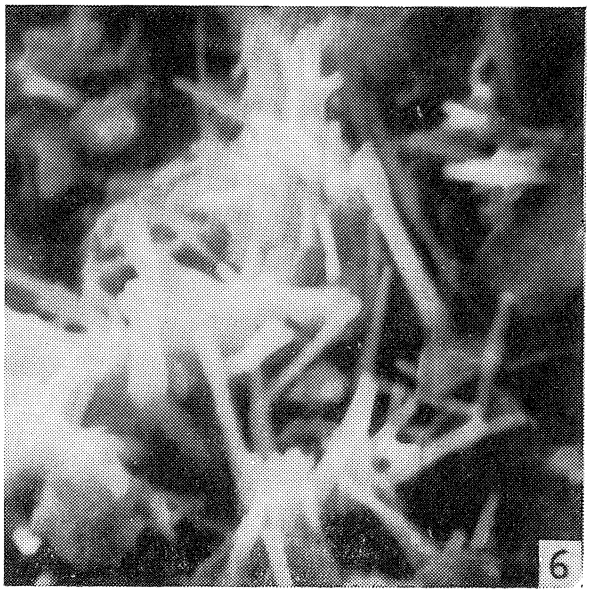
6

PLATE — PLANSZA II

Fig. 1. Calcidetritic sandstone gradually (inwards of nodule) replaced by oligonite aggregate. Contemporaneously, interstitial clay minerals transform into Fe-septechlorite-rich segregations, excluding coarser detritic white hydromica. Bukowiec 20. Thin section, × 10

Fig. 1. Wapienno-detrytyczny piaskowiec, stopniowo (do środka konkrecji) zastępowany przez agregat oligonitowy. Równocześnie intersticjalne minerały ilaste przeobrażają się w segregacje Fe-septechlorytowe, za wyjątkiem grubiej detrytycznej jasnej hydromiki. Bukowiec 20. Płytka cienka, × 10

Fig. 2. Partly oxidized and hydrated rhodochrosite permeates almost completely burrowing traces in fine-grained rhodochrosite-francolite nodule, Dąbrówka 22. Thin section, × 10

Fig. 2. Częściowo utleniony i uwodniony rodochrozyt przepaja niemal całkowicie ślady żerowania w drobnoziarnistej konkrecji rodochrozytowo-frankolitowej. Dąbrówka 22. Płytka cienka, × 10

PLATE — PLANSZA III

Fig. 1. Cellular structure of ferromanganese-oxide nodule. The cell walls are symmetrically built from center by: pyrolusite (white), goethite, and hematite + goethite (dark-grey). The cell interiors being partly filled by finely dispersed hydrous Fe-Mn oxides (single goethite lines in X-ray powder pattern) exhibit botryoidal surface of colloform aggregates. Lachowice 9. Polished section. × 2

Fig. 1. Komórkowa budowa konkrecji żelazomanganowo-tlenkowej. Ściany komór są symetrycznie zbudowane od środka na zewnątrz przez: piroluzyt (biały), goethyt, hematyt + goethyt (ciemnoszary). Wnętrza komór będąc w części wypełnione drobnodyspersyjnymi wodnymi tlenkami Fe-Mn (pojedyncze linie goethytu w rentgenowskich obrazach proszkowych) ujawniają gronkowate powierzchnie agregatów kollomorficznych. Lachowice 9. Zgład polerowany, × 2

Fig. 2. Ferromanganese-oxide nodule of similar origin and composition (further explanations, see Fig. 1 and in text). Lachowice 15. Polished section, × 2

Fig. 2. Podobnie powstała i złożona konkrecja żelazomanganowo-tlenkowa (dalsze objaśnienia p. Fig. 1 i w tekście). Lachowice 15. Zgład polerowany, × 2

PLATE — PLANSZA IV

Fig. 1. The surface of the cavity in the interior of the ferromanganeseoxide nodule. Undetermined organic remnants fossilized by hydrous Fe-Mn oxides of colloform structure are well discernable. Tarnawa Górna 7. Scanning electron micrograph (Stereoscan S4-10), × 500

Fig. 1. Powierzchnia próżni we wnętrzu konkrecji żelazomanganowo-tlenkowej. Dobrze rozpoznawalne nieokreślone szczątki organiczne, sfossylizowane wodnymi tlenkami Fe-Mn o budowie kollomorficznej. Tarnawa Górna 7. Zdjęcie mikroskopem skanningowym (Stereoscan S4-10), × 500

Fig. 2. As above. Magnification × 2100

Fig. 2. Jak wyżej. Powiększenie × 2100

Fig. 3. Clusters of todorokite fibers on the fracture surface in external part of the ferromanganese nodule. Ostrósza 6. Scanning electron micrograph, × 2100

Fig. 3. Grupki włókien todorokitu na powierzchni przełamowej w zewnętrznej części konkrecji żelazomanganowej. Ostrósza 6. Zdjęcie mikroskopem skanningowym, × 2100

Fig. 4. As above. Magnification × 5200

Fig. 4. Jak wyżej. Powiększenie × 5200

Fig. 5. Dispersed todorokite fibers on the fracture surface in external part of the ferromanganese nodule. Ostrósza 6. Scanning electron micrograph, × 2200

Fig. 5. Rozproszone włókna todorokitu na powierzchni przełamowej w zewnętrznej części konkrecji żelazomanganowej. Ostrósza 6. Zdjęcia mikroskopem skanningowym, × 2200

Fig. 6. As above. Magnification × 5500

Fig. 6. Jak wyżej. Powiększenie × 5500